Geophys. J. R. astr. Soc. (1976) **47**, 97–133

Potentials and displacements for two theoretical seismic sources

David G. Harkrider *Seismological Laboratory, Division of Geological and Planetary Sciences, California Institute of Technology, Pasadena, California 91125, USA*

Received 1976 April 22; in original form 1975 August 21

Summary. Theoretical, *P*, *SV*, and *SH* displacement potentials and displacements for a double couple or point shear dislocation source and for a 'mixed-quadrupole' source at any arbitrary orientation in an isotropic homogeneous elastic space are expressed as multiple integral and derivative operations on the source history in the time domain and their algebraic equivalent in the frequency domain. These sources have the same angle orientation functions, which are given explicitly. The double couple and 'mixed quadrupole' are both quadrupole sources but, unlike the double couple, the *P* and *S* waves from a 'mixed quadrupole' have different source histories. Analytic displacements are obtained using as examples the Ohnaka shear dislocation history for a double couple and the Randall and Archambeau tectonic release histories for 'mixed quadrupole' sources.

The displacement fields are investigated numerically, in order to establish a criterion for estimating the minimum range for applying far-field theory results to the total displacement field. The chosen criterion is the ratio of the far-field peak amplitude, which is a function of source rise or duration time, to the static displacement, which is a near-field phenomenon. The proposed criterion is found to be conservative as to the minimum range for the far-field, predicted $(1/R)$ dependence of the total field peak amplitude, but quite satisfactory for time domain estimates of moment and corner frequency based on far-field theory.

Introduction

Sato (1972) presented compact integral representations in separable cylindrical coordinates for the compressional and cylindrical shear displacement potentials for a double couple of arbitrary orientation in a homogeneous isotropic elastic space. These were obtained by combining his integral representations for dip-slip faults and strike-slip faults with arbitrary dip angles (Sato 1969). The double couple integral representations of cylindrical shear potentials appropriate for the dip- and strike-slip fault models were derived from the integral representations of the Cartesian shear potentials. In this paper, the same integral representations

for the compressional and cylindrical shear potentials for a double couple of arbitrary orientation are obtained by directly comparing the integral representation of the cylindrical components of the displacement field with the operational representation of cylindrical displacements in terms of the compressional and cylindrical shear potentials. These results are extended to include closed form solutions for the potentials which can be transformed into the time domain by inspection.

Although they are more awkward than cylindrical potentials when used in a multilayer formulation, the Cartesian shear potentials can be readily expressed in terms of spherical harmonics and are easily evaluated from a known displacement field. These two properties of Cartesian potentials make it possible to use the results of near-field finite difference or finite element calculations to find the far-field waves generated by an arbitrary finite non-linear source. In this paper, we give some general relations between the two types of shear potentials but restrict the results to our two classes of quadrupoles of arbitrary orientation.

Cartesian potentials are then used to obtain closed form solutions of the spherical components of the total displacement field. While the derivations are for a double couple, or point shear, dislocation, the expressions are readily applicable to a second class of quadrupoles of seismic interest, the 'mixed quadrupole', where the compressional and shear waves have different source histories.

The total time-domain total displacement fields due to a double couple and 'mixed quadrupole' are investigated numerically for the purpose of determining a criterion for estimating the minimum range for neglecting the near-field contribution to displacement in terms of source duration. The Ohnaka (1973) dislocation time history is used for the double couple source and the Randall (1966) and Archambeau (1972) finite-volume tectonic release histories are used for the mixed quadrupole sources. The estimates of minimum range of far-field applicability in the time domain are evaluated in terms of seismic moment error and $(1/R)$ peak amplitude variation. The possibility of time-domain estimates of spectral corner frequency are discussed for the assumed time histories.

Shear fault-dislocation source

One of the fault models considered by Haskell (1964) was the shear fault in which the displacements parallel to the fault plane are discontinuous across the fault surface. He showed that the radiated displacement fields are exactly the same as those that one would observe by considering the fault plane to be covered by a distribution of double couple sources whose normals lie in the fault plane.

Most of this section will be restricted to the horizontal double couple appropriate for a vertical strike slip fault distribution. Expressions for double couples corresponding to fault planes of arbitrary dip and slip angle are given in the Appendices. In the first part of this section, the frequency-domain cylindrical displacement and potential fields are obtained as integrals over the horizontal wave number. Next, the integral expressions are evaluated to obtain frequency-domain solutions. Frequency-domain closed form solutions are then given for the Cartesian potentials and spherical displacements in spherical harmonics. Finally the spherical components of the total displacement field are derived for the time domain in terms of derivatives and integrals of the dislocation history and a particular dislocation time history is chosen for numerical examples.

INTEGRAL SOLUTIONS FOR CYLINDRICAL DISPLACEMENTS AND POTENTIALS

Taking the Fourier-time transform of the Cartesian displacements due to a horizontal double couple or the integrand of the fault surface integral (Haskell 1964; Burridge, Lapwood &

Knopoff 1964) we obtain

$$\bar{u}(\omega, \mathbf{r}) = -\frac{\mu \bar{D}(\omega)}{4\pi\rho\omega^2}\left\{\frac{2\partial^3(A_\beta - A_\alpha)}{\partial x_i \partial x_1 \partial x_2} + k_\beta^2\left(\delta_{i1}\frac{\partial}{\partial x_2} + \delta_{i2}\frac{\partial}{\partial x_1}\right)A_\beta\right\} \tag{1}$$

where

(x_1, x_2, x_3) = Cartesian coordinates at which $\bar{u}_i$ is to be evaluated,

$$A_v = \frac{\exp(-ik_v R)}{R},$$

$$\bar{D}(\omega) = \int_{-\infty}^{\infty} D(t)\exp(-i\omega t)\,dt,$$

$D(t)$ = relative displacement time history across the fault plane,
$k_v = \omega/v$,
v = seismic body velocity, either the compressional velocity, α, or the shear velocity, β,
$\mathbf{r}$ = position vector from source to observer, and
$R = |\mathbf{r}|$, the distance from source to observer.

The remaining undefined quantities in equation (1) are given in Haskell (1964). The source orientation is such that the double couple arms are parallel to the x_1 and x_2 coordinates and centred at $(0, 0, h)$.

It should be emphasized that the displacements and potentials that follow are the integrands of a surface integral over the fault plane unless otherwise specified. They can be converted to true displacements and potentials due to a point double couple by replacing $\mu\bar{D}(\omega)$ with the spectral moment $\bar{M}(\omega)$.

The cylindrical displacements $(\bar{q}, \bar{v}, \bar{w})$ in the (r, ϕ, z) cylindrical coordinate system are given by

$$\bar{q} = \frac{\partial x_i}{\partial r}\bar{u}_i = -\mu\frac{\bar{D}(\omega)}{4\pi\rho\omega^2}\sin 2\phi\left\{\frac{\partial}{\partial r}\left[\frac{\partial^2}{\partial r^2} - \frac{1}{r}\frac{\partial}{\partial r}\right](A_\beta - A_\alpha) + k_\beta^2\frac{\partial A_\beta}{\partial r}\right\}$$

$$\bar{v} = \frac{1}{r}\frac{\partial x_i}{\partial \phi}\bar{u}_i = -\mu\frac{\bar{D}(\omega)}{4\pi\rho\omega^2}\cos 2\phi\left\{\frac{2}{r}\left[\frac{\partial^2}{\partial r^2} - \frac{1}{r}\frac{\partial}{\partial r}\right](A_\beta - A_\alpha) + \frac{\partial A_\beta}{\partial r}\right\}$$

$$\bar{w} = \frac{\partial x_i}{\partial z}\bar{u}_i = -\mu\frac{\bar{D}(\omega)}{4\pi\rho\omega^2}\sin 2\phi\left\{\frac{\partial}{\partial z}\left[\frac{\partial^2}{\partial r^2} - \frac{1}{r}\frac{\partial}{\partial r}\right](A_\beta - A_\alpha)\right\}. \tag{2}$$

In cylindrical coordinates, the displacements can also be written in potential form as

$$\bar{\mathbf{u}} = \operatorname{grad}\bar{\Phi} + \operatorname{curl}\operatorname{curl}(0, 0, \bar{\Psi}) + \operatorname{curl}(0, 0, \bar{X}) \tag{3}$$

or

$$\bar{q} = \frac{\partial\bar{\Phi}}{\partial r} + \frac{\partial^2\bar{\Psi}}{\partial r\partial z} + \frac{1}{r}\frac{\partial\bar{X}}{\partial\phi}$$

$$\bar{v} = \frac{1}{r}\frac{\partial\bar{\Phi}}{\partial\phi} + \frac{1}{r}\frac{\partial^2}{\partial z\partial\phi}\bar{\Psi} - \frac{\partial\bar{X}}{\partial r}$$

$$\bar{w} = \frac{\partial\bar{\Phi}}{\partial z} + \frac{\partial^2\bar{\Psi}}{\partial z^2} + k_\beta^2\bar{\Psi}. \tag{4}$$

The potential relation for $\bar{w}$ was obtained by also making use of the fact that the individual potentials satisfy their respective time-transformed scalar wave equations, i.e. scalar Helmholtz equations.

Using the Sommerfeld integral representation

$$\frac{\exp(-ik_v R)}{R} = \int_0^\infty F_v J_0(kr)\,dk \tag{5}$$

where

$$F_v = \frac{k \exp(-\nu_v |z-h|}{\nu_v}$$

$$\nu_v = \begin{cases} (k^2 - k_v^2)^{1/2}; & k > k_v \\ i(k_v^2 - k^2)^{1/2}; & k < k_v \end{cases}$$

for substitution in equation (2) and comparing with the potential form, equation (4), we have

$$\bar{\Phi} = \mu \frac{\bar{D}(\omega)}{4\pi\rho\omega^2} \sin 2\phi \int_0^\infty k^2 F_\alpha J_2(kr)\,dk \tag{6a}$$

$$\bar{\Psi} = \mu \frac{\bar{D}(\omega)}{4\pi\rho\omega^2} \sin 2\phi \int_0^\infty \mathrm{sgn}(z-h)\,\nu_\beta F_\beta J_2(kr)\,dk \tag{6b}$$

$$\bar{X} = -\mu \frac{\bar{D}(\omega)}{4\pi\rho\omega^2} \cos 2\phi \int_0^\infty k_\beta^2 F_\beta J_2(kr)\,dk. \tag{6c}$$

Equations (6) can also be found in Sato (1969, 1972) for the double couple orientation of (90°, 0°), i.e. $\delta = 90°$ and $\lambda = 0$. Relations corresponding to equations (2) and (6) for the double couple of arbitrary orientation (δ, λ), Fig. 1, are given in Appendix A.

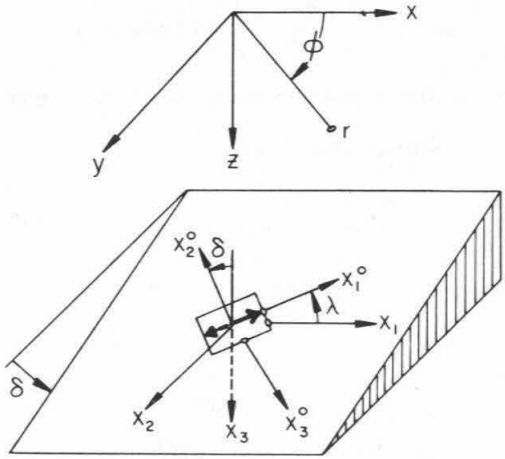

Figure 1. Spatial parameters of a dislocation source.

In Appendix A we see that the displacement field for any orientation of a double couple is the sum of displacement fields of three particular orientations of the double couple. This often-stated observation involves the displacement fields of the double couples corresponding to the normal strike-slip fault (90°, 0), normal dip-slip fault (90°, 90°), and the dip-slip fault with a 45° dip (45°, 90°), e.g. Burridge *et al.* (1964) and Ben-Menahem & Singh (1968). The combination of the displacement fields for the first two faults is straightforward, but the use of the displacement fields for the last fault requires some care in that the third fundamental displacement fields are the displacements observed at an azimuth angle of 45° from the strike of the fault. This is because the displacement fields for this fault orientation also contain a contribution from the fundamental displacements corresponding to a normal strike-slip fault with an azimuthal dependence of $\cos 2\phi$ for the vertical and radial components and a dependence of $\sin 2\phi$ for the azimuthal component. With the replacement of $\cos 2\phi$ by $-\sin 2\phi$, the azimuthal displacements for the normal strike slip and the dip slip with 45° dip are identical.

From Appendix A, the cylindrical potentials for the three faults are as follows:

Normal dip-slip:

$$\bar{\Phi} = -\mu \frac{\bar{D}(\omega)}{4\pi\rho\omega^2} 2 \sin\phi \int_0^\infty \operatorname{sgn}(z-h)\, k\nu_\alpha J_1(kr) F_\alpha \, dk$$

$$\bar{\Psi} = -\mu \frac{\bar{D}(\omega)}{4\pi\rho\omega^2} \sin\phi \int_0^\infty \frac{2k^2 - k_\beta^2}{k} J_1(kr) F_\beta \, dk$$

$$\bar{X} = \mu \frac{\bar{D}(\omega)}{4\pi\rho\omega^2} \cos\phi \int_0^\infty k_\beta^2 \operatorname{sgn}(z-h) \frac{\nu_\beta}{k} J_1(kr) F_\beta \, dk. \tag{7}$$

Dip-slip with 45° dip:

$$\bar{\Phi} = \mu \frac{\bar{D}(\omega)}{4\pi\rho\omega^2} \frac{1}{2} \int_0^\infty \{(k^2 + 2\nu_\alpha^2) J_0(kr) + k^2 \cos 2\phi J_2(kr)\} F_\alpha \, dk$$

$$\bar{\Psi} = \mu \frac{\bar{D}(\omega)}{4\pi\rho\omega^2} \frac{1}{2} \int_0^\infty \operatorname{sgn}(z-h) \nu_\beta \{3J_0(kr) + \cos 2\phi J_2(kr)\} F_\beta \, dk$$

$$\bar{X} = \mu \frac{D(\omega)}{4\pi\rho\omega^2} \int_0^\infty k_\beta^2 \sin 2\phi J_2(kr) F_\beta \, dk. \tag{8}$$

The potentials for the normal strike slip were given in equation (6). Although the three fundamental fields were determined by inspection of the displacement fields from an arbitrary double couple orientation, they can also be obtained from the potential relations (Sato 1969, 1972).

FREQUENCY DOMAIN CLOSED FORM SOLUTIONS FOR CYLINDRICAL POTENTIALS

In the integral solutions of equations (6), (7) and (8), all of the integral forms but two are frequently found in the geophysical literature and involve differentiation of the Sommerfeld

integral. The other two integral forms I_v and S_v where

$$I_v = \int_0^\infty F_v J_2(kr)\, dk$$

and

$$S_v = \int_0^\infty F_v \frac{J_1(kr)}{k}\, dk \tag{9}$$

are related to each other in terms of the Sommerfeld integral by

$$I_v = -\int_0^\infty F_v J_0(kr)\, dk + \frac{2}{r} S_v \tag{10}$$

or

$$I_v = -\frac{\exp(-ik_v R)}{R} + \frac{2}{r} S_v$$

The closed form of S_v can be found in Erdelyi *et al.* (1954), Laplace transform 4.15 (13) just below the Sommerfeld integral. Changing the variable of integration, we obtain

$$S_v = \frac{1}{ik_v r} \left[\exp(-ik_v |z-h|) - \exp(-ik_v R)\right] \tag{11}$$

and by equation (10)

$$I_v = -\frac{\exp(-ik_v R)}{R} + \frac{2}{ik_v r^2} \left[\exp(-ik_v |z-h|) - \exp(-ik_v R)\right]. \tag{12}$$

It should be noted that the S_v and I_v terms contribute near field terms to the cylindrical shear potentials which are non-causal in a propagation sense. This can be seen from the imaginary exponentials involving $|z-h|$, which represent plane phase waves travelling in the z direction away from the source. When these potentials are used to calculate the total displacement field, the non-causal terms are eliminated.

Because of the unfamiliar form of (S_v/r), which will appear in our potentials, we give its asymptotic values for vanishing r and ω.

$$\lim_{r \to 0} \left(\frac{S_v}{r}\right) = \frac{\exp(-ik_v |z-h|)}{2|z-h|} \tag{13a}$$

$$\lim_{\omega \to 0} \left(\frac{S_v}{r}\right) = \frac{1}{r^2} (R - |z-h|). \tag{13b}$$

Equation (13b) is compatible with (13a) as $\omega \to 0$, since for $r \ll |z-h|$

$$R \cong |z-h| + \frac{1}{2} \frac{r^2}{|z-h|}.$$

The closed form solutions for the potentials associated with the three fault orientations

are

Normal strike-slip:

$$\bar{\Phi} = -\mu \frac{\bar{D}(\omega)}{4\pi\rho\omega^2} \left\{k_\alpha^2 - \frac{3(1+ik_\alpha R)}{R^2}\right\} A_\alpha \frac{r^2}{R^2} \sin 2\phi$$

$$\bar{\Psi} = \mu \frac{\bar{D}(\omega)}{4\pi\rho\omega^2} \left\{(h-z) \frac{(1+ik_\beta R)}{R^2} A_\beta + \frac{2}{r^2} [\operatorname{sgn}(z-h) \exp(-ik_\beta|z-h|) - (z-h)A_\beta]\right\} \sin 2\phi$$

$$\bar{X} = \mu \frac{D(\omega)}{4\pi\rho\omega^2} k_\beta^2 \left\{A_\beta - \frac{2}{r} S_\beta\right\} \cos 2\phi. \tag{14}$$

Normal dip-slip:

$$\bar{\Phi} = \mu \frac{\bar{D}(\omega)}{4\pi\rho\omega^2} 2\left\{k_\alpha^2 - \frac{3(1+ik_\alpha R)}{R^2}\right\} A_\alpha \frac{(z-h)}{R^2} \sin\phi$$

$$\bar{\Psi} = -\mu \frac{\bar{D}(\omega)}{4\pi\rho\omega^2} \left\{\frac{2(1+ik_\beta R)}{R^2} A_\beta - k_\beta^2 \frac{S_\beta}{r}\right\} r \sin\phi$$

$$\bar{X} = -\mu \frac{\bar{D}(\omega)}{4\pi\rho\omega^2} \frac{k_\beta^2}{r} \{(z-h)A_\beta - \operatorname{sgn}(z-h) \exp(-ik_\beta|z-h|)\} \cos\phi. \tag{15}$$

Dip-slip with 45° dip:

$$\bar{\Phi} = -\mu \frac{\bar{D}(\omega)}{4\pi\rho\omega^2} \frac{1}{2} \left\{\left[k_\alpha^2 - \frac{3(1+ik_\alpha R)}{R^2}\right] A_\alpha \left[\frac{3(z-h)^2}{R^2} - 1 + \frac{r^2}{R^2} \cos 2\phi\right]\right\}$$

$$\bar{\Psi} = \mu \frac{\bar{D}(\omega)}{4\pi\rho\omega^2} \frac{1}{2} \left\{\frac{(1+ik_\beta R)}{R} A_\beta \frac{(z-h)}{R} (3 - \cos 2\phi) + \frac{2}{r^2} [\operatorname{sgn}(z-h) \exp(-ik_\beta|z-h|) - (z-h)A_\beta] \cos 2\phi\right\}$$

$$\bar{X} = -\mu \frac{\bar{D}(\omega)}{4\pi\rho\omega^2} k_\beta^2 \left\{A_\beta - \frac{2}{r} S_\beta\right\} \sin 2\phi. \tag{16}$$

The compressional and azimuthal shear potentials are the same as those given in Helmberger (1974) except for a factor equal to the fault area. His results are obtained by integrating the dislocation over the fault surface and neglecting the phase variation over the surface. His definition of the vertical shear potential differs from ours, but is consistent.

The normal dip-slip potentials are different in sign from those of Helmberger (1974) since he assumes that the positive ϕ face of the fault moved in the positive z direction or downward with respect to the negative ϕ fault face. This corresponds in our geometry to a $(90°, -90°)$ fault orientation.

INTEGRAL SOLUTIONS FOR CARTESIAN POTENTIALS

The cylindrical shear potentials discussed in the previous sections are especially useful in problems with cylindrical symmetry such as elastic-wave propagation in a piecewise

homogeneous model of a vertically heterogeneous half space. This results not only from their symmetry but also because there are only two shear potentials, an SV and an SH while there are three Cartesian shear potentials. The integral forms of the potentials facilitate their application to multilayer formulations for body waves (Helmberger 1974) and surface waves since their integrands involve terms common to this type of formulation (Harkrider & Archambeau, in preparation). In discussing body waves from sources in whole spaces, the cylindrical potentials have the disadvantage in that they are frequently non-causal. This non-causal near-field wave is an artefact due to the definition of the potentials and is not present in the displacement field solution. Since the usual definition of Cartesian potentials is related to simple physical operations on the displacement field such as the curl (or the rotation) of the field, they are not only causal in a propagation sense, but are useful in multipole representations of sources for which the displacement field is a direct result of the formulation, i.e. a potential formulation is not used. The latter is especially advantageous to numerical finite difference or finite element methods which are now being applied to simulate the non-linear processes at the source.

The resolution of the displacement field into Cartesian potentials is given by

$$\bar{\mathbf{u}} = \operatorname{grad} \bar{\Phi} + \operatorname{curl} (\bar{\psi}_1, \bar{\psi}_2, \bar{\psi}_3) \tag{17}$$

with the additional requirement that

$$\operatorname{div} (\bar{\psi}_1, \bar{\psi}_2, \bar{\psi}_3) = 0. \tag{18}$$

It is this last requirement that makes the shear potentials $(\bar{\psi}_1, \bar{\psi}_2, \bar{\psi}_3)$ have a simple relation to the rotation components of the displacement field.

The cylindrical potentials can also be put in the Cartesian form of equation (26), i.e.

$$\bar{\mathbf{u}} = \operatorname{grad} \bar{\Phi} + \operatorname{curl} (\tilde{\psi}_1, \tilde{\psi}_2, \tilde{\psi}_3) \tag{19}$$

where performing the curl operation in equation (3), transforming the resulting vector into its Cartesian components, and comparing with equation (28), we obtain (Takeuchi 1966)

$$\begin{aligned} \tilde{\psi}_1 &= \frac{\partial \bar{\Psi}}{\partial y} \\ \tilde{\psi}_2 &= -\frac{\partial \bar{\Psi}}{\partial x} \\ \tilde{\psi}_3 &= \bar{X} \end{aligned} \tag{20}$$

and the scalar compressional potentials, $\bar{\Phi}$, are identical. Performing the divergence of the vector shear potential components of equation (20), we obtain

$$\operatorname{div} (\tilde{\psi}_1, \tilde{\psi}_2, \tilde{\psi}_3) = \frac{\partial \bar{X}}{\partial z}. \tag{21}$$

The Cartesian components of both sets of vector shear potentials satisfy the scalar Helmholtz equation in the frequency domain and the scalar-wave equation in the time domain. Thus the vector potentials satisfy the vector Helmholtz equation

$$\nabla^2 \bar{\boldsymbol{\psi}} = -k_\beta^2 \bar{\boldsymbol{\psi}} \tag{22}$$

where

$$\nabla^2 \bar{\psi} \equiv \text{grad div } \bar{\psi} - \text{curl curl } \bar{\psi}$$

$$\equiv \nabla(\nabla \cdot \bar{\psi}) - \nabla \times \nabla \times \bar{\psi}$$

The cylindrical components of the vector, $\bar{\psi}$, in equation (22) do not satisfy scalar Helmholtz equations. This is the reason in cylindrical symmetry problems for introducing the scalar cylindrical shear potentials. $\bar{\Psi}$ and $\bar{X}$, which do satisfy the scalar equations.

Since we are going to eventually discuss the solutions for a whole space, we will restrict the following to the solutions due to the double couple appropriate for a normal strike-slip fault. As stated previously, the Cartesian shear potentials are primarily useful in whole space problems where the orientation of the coordinate system is arbitrary.

Performing the operations in equation (20), we obtain for the Cartesian components of the vector shear potential, $\tilde{\bar{\psi}}$,

$$\tilde{\bar{\psi}}_1 = \frac{\mu \bar{D}(\omega)}{4\pi\rho\omega^2} \frac{1}{2} \int_0^\infty \text{sgn}(z-h)\, k\nu_\beta F_\beta \{\cos\phi J_1(kr) + \cos 3\phi J_3(kr)\}\, dk$$

$$\tilde{\bar{\psi}}_2 = -\frac{\mu \bar{D}(\omega)}{4\pi\rho\omega^2} \frac{1}{2} \int_0^\infty \text{sgn}(z-h)\, k\nu_\beta F_\beta \{\sin\phi J_1(kr) - \sin 3\phi J_3(kr)\}\, dk$$

$$\tilde{\bar{\psi}}_3 = \bar{X} = -\frac{\bar{D}(\omega)}{4\pi} \cos 2\phi \int_0^\infty F_\beta J_2(kr)\, dk. \tag{23}$$

By inspection of the integrands of equation (23), we see that the three Cartesian components are indeed solutions of the scalar-shear Helmholtz equation. This follows from relation (20) since Cartesian derivatives of solutions to the scalar Helmholtz equation are also solutions. It should be noted that these components also contain the 'non-causal' near-field wave.

In Appendix B, the Cartesian components of the 'causal' vector shear potential, $\bar{\bar{\psi}}$, are shown to be related to Cartesian components of the 'non-causal' shear vector potential, $\tilde{\bar{\psi}}$, by

$$\bar{\bar{\psi}}_1 = \tilde{\bar{\psi}}_1 + \frac{1}{k_\beta^2} \frac{\partial^2 \tilde{\bar{\psi}}_3}{\partial x \partial z}$$

$$\bar{\bar{\psi}}_2 = \tilde{\bar{\psi}}_2 + \frac{1}{k_\beta^2} \frac{\partial^2 \tilde{\bar{\psi}}_3}{\partial y \partial z}$$

$$\bar{\bar{\psi}}_3 = \tilde{\bar{\psi}}_3 + \frac{1}{k_\beta^2} \frac{\partial^2 \tilde{\bar{\psi}}_3}{\partial z^2}. \tag{24}$$

Substituting equations (23) into equations (24), we obtain the Cartesian components of the 'physical' or 'causal' vector shear potential in integral form

$$\bar{\psi}_1 = \frac{\mu \bar{D}(\omega)}{4\pi\rho\omega^2} \cos\phi \int_0^\infty \operatorname{sgn}(z-h)\, k\nu_\beta F_\beta J_1(kr)\, dk$$

$$\bar{\psi}_2 = -\frac{\mu \bar{D}(\omega)}{4\pi\rho\omega^2} \sin\phi \int_0^\infty \operatorname{sgn}(z-h)\, k\nu_\beta F_\beta J_1(kr)\, dk$$

$$\bar{\psi}_3 = -\frac{\mu \bar{D}(\omega)}{4\pi\rho\omega^2} \cos 2\phi \int_0^\infty k^2 F_\beta J_2(kr)\, dk. \tag{25}$$

Components $\bar{\psi}_1$ and $\bar{\psi}_2$ can also be written as

$$\bar{\psi}_1 = -\frac{\mu \bar{D}(\omega)}{4\pi\rho\omega^2} \cos\phi \frac{\partial}{\partial z} \int_0^\infty kF_\beta J_1(kr)\, dk$$

$$\bar{\psi}_2 = \frac{\mu \bar{D}(\omega)}{4\pi\rho\omega^2} \sin\phi \frac{\partial}{\partial z} \int_0^\infty kF_\beta J_1(kr)\, dk. \tag{26}$$

As we will see in a later section, in order for integrals over k to be 'causal', i.e. to be represented by a finite number of space derivatives of the Summerfeld integral or a finite number of spherical harmonics, it is sufficient that the integral be of the form

$$\int_0^\infty k^n F_\upsilon J_n(kr)\, dk.$$

For $n = 0$, this is the form of the Sommerfeld integral. From inspection of equations (6), (25) and (26) we see that the compressional or P potential, $\bar{\Phi}$, and the Cartesian components of the vector shear potential ($\bar{\psi}_1$, $\bar{\psi}_2$, $\bar{\psi}_3$) are all 'causal'.

The 'non-causal' vector shear potential resolution ($\tilde{\psi}_1$, $\tilde{\psi}_2$, $\tilde{\psi}_3$) was used to obtain the 'causal' vector resolution ($\bar{\psi}_1$, $\bar{\psi}_2$, $\bar{\psi}_3$) in integral form. Other than that, it has very little practical use. On the other hand the scalar cylindrical shear potentials $\bar{\Psi}$ and $\bar{X}$, even though sometimes 'non-causal', are important in vertically heterogeneous half-space formulations. They can be obtained directly from ($\bar{\psi}_1$, $\bar{\psi}_2$, $\bar{\psi}_3$) by the integrand relations (Harkrider & Archambeau, in preparation).

$$\bar{\bar{\Psi}} = \frac{1}{k^2}\left(\frac{\partial \bar{\bar{\psi}}_2}{\partial x} - \frac{\partial \bar{\bar{\psi}}_1}{\partial y}\right)$$

and

$$\bar{\bar{X}} = \frac{k_\beta^2}{k^2}\, \bar{\bar{\psi}}_3 \tag{27}$$

where we have used the implicit notation definition

$$\bar{\psi}_1 = \int_0^\infty \bar{\bar{\psi}}_1\, dk, \text{ etc.}$$

The latter of equations (27) follows directly from the last relation of equations (24), since $\bar{X} \equiv \tilde{\psi}_3$ and

$$\frac{\partial^2}{\partial z^2}\, \bar{\bar{X}} = -\nu_\beta^2 \bar{\bar{X}} = (k_\beta^2 - k^2)\, \bar{\bar{X}} \tag{28}$$

as a result of satisfying the scalar Helmholtz equation.

FREQUENCY DOMAIN CLOSED FORM SOLUTIONS FOR CARTESIAN POTENTIALS

Since the Cartesian components of the vector shear potential $(\bar{\psi}_1, \bar{\psi}_2, \bar{\psi}_3)$ are simply related to the Cartesian components of the rotation vector, $\boldsymbol{\Omega}$, of the displacement field by

$$\bar{\Omega}_i = \frac{k_\beta^2}{2}\,\bar{\psi}_i; \qquad i = 1, 2, 3 \tag{29}$$

where

$$\boldsymbol{\Omega} \equiv \tfrac{1}{2}\,\mathrm{curl}\,\mathbf{u} \tag{30}$$

the closed form Cartesian components of the vector shear potential can easily be obtained by performing the operation given in equations (29) and (30) on the known source displacement field, i.e.

$$\bar{\psi}_i = \frac{1}{k_\beta^2}\,\mathrm{curl}\,\bar{\mathbf{u}}. \tag{31}$$

Similarly the compressional wave potential, $\bar{\Phi}$, may be obtained by the operation

$$\bar{\Phi} = -\frac{1}{k_\alpha^2}\,\mathrm{div}\,\bar{\mathbf{u}}. \tag{32}$$

By applying equations (32) and (31) to equations (1) we obtain

$$\bar{\Phi} = \frac{\mu\bar{D}(\omega)}{4\pi\rho\omega^2}\,\frac{2\partial^2 A_\alpha}{\partial x\partial y}$$

$$\bar{\psi}_1 = \frac{\mu\bar{D}(\omega)}{4\pi\rho\omega^2}\,\frac{\partial^2 A_\beta}{\partial x\partial z}$$

$$\bar{\psi}_2 = -\frac{\mu\bar{D}(\omega)}{4\pi\rho\omega^2}\,\frac{\partial^2 A_\beta}{\partial y\partial z}$$

$$\bar{\psi}_3 = -\frac{\mu\bar{D}(\omega)}{4\pi\rho\omega^2}\left\{\frac{\partial^2 A_\beta}{\partial x^2} - \frac{\partial^2 A_\beta}{\partial y^2}\right\} \tag{33}$$

We could have obtained equations (33) directly from equations (6a), (25) and (26) by comparison with relations for the Cartesian derivatives of the Sommerfeld integral. It is easy to verify that equations (33) yield equations (1) when substituted in equation (17) and that $\mathrm{div}\,(\bar{\psi}_1, \bar{\psi}_2, \bar{\psi}_3) = 0$.

We next express the Cartesian potentials $\bar{\Phi}$ and $(\bar{\psi}_1, \bar{\psi}_2, \bar{\psi}_3)$ in terms of spherical harmonics and spherical Bessel functions. This is done by applying the following result due to Erdélyi (1937) and Ben-Menahem & Singh (1968) to the integral solutions of the potentials:

$$h_n^{(2)}(k_\upsilon R)\,P_n^m(\cos\theta) = \frac{i^{m+1-n}}{k_\upsilon}\,\epsilon^{m+n}\int_0^\infty \left(\frac{k}{k_\upsilon}\right)^m P_n^{(m)}\{i\nu_\upsilon/k_\upsilon\}\,F_\upsilon\,J_m(kr)\,dk \tag{34}$$

where

$$\epsilon = \operatorname{sgn}(z-h)$$

$$P_n^m(\cos\theta) = (\sin\theta)^m P_n^{(m)}(\cos\theta)$$

$$P_n^{(m)}(x) \equiv \frac{d^m}{dx^m} P_n(x)$$

and

$$h_n^{(2)}(x) = i(-1)^n x^n \left(\frac{d}{x\,dx}\right)^n \frac{\exp(-ix)}{x}. \tag{35}$$

Thus equations (6a), (25) and (26) can be written as

$$\bar{\Phi} = -i\frac{\mu\bar{D}(\omega)}{4\pi\rho\omega^2} k_\alpha^3 \sin^2\theta \sin 2\phi\, h_2^{(2)}(k_\alpha R)$$

$$\bar{\psi}_1 = -i\frac{\mu\bar{D}(\omega)}{4\pi\rho\omega^2} k_\beta^3 \cos\theta \sin\theta \cos\phi\, h_2^{(2)}(k_\beta R)$$

$$\bar{\psi}_2 = i\frac{\mu\bar{D}(\omega)}{4\pi\rho\omega^2} k_\beta^3 \cos\theta \sin\theta \sin\phi\, h_2^{(2)}(k_\beta R)$$

$$\bar{\psi}_3 = i\frac{\mu\bar{D}(\omega)}{4\pi\rho\omega^2} k_\beta^3 \sin^2\theta \cos 2\phi\, h_2^{(2)}(k_\beta R) \tag{36}$$

where we have used

$$P_2^{(1)}\{iv_v/k_v\} = 3iv_v/k_v$$

$$P_2^{(2)}\{iv_v/k_v\} = 3$$

$$P_2^1(\cos\theta) = 3\sin\theta\cos\theta$$

and

$$P_2^2(\cos\theta) = 3\sin^2\theta. \tag{37}$$

The Cartesian potentials for any arbitrary orientation are given in Appendix A.

Equations (36) are in the same form as the Cartesian potentials given by Archambeau (1972) for the tectonic release source. This allows us to make a direct correspondence between his coefficients and ours. We then can apply the double couple relations, with trivial modifications to the general class of 'mixed quadrupoles' of which his is an example. In particular, the orientation angle functions for the spherical components of displacement are the same for both classes of seismic sources and can be found in Appendix C.

FREQUENCY DOMAIN CLOSED FORM SOLUTIONS FOR SPHERICAL DISPLACEMENTS

Converting equations (36) into spherical components of the vector shear potential and making use of the Helmholtz resolution, we obtain the following spherical displacements for P and S waves generated by a horizontal double couple.

P-wave:

$$\bar{u}_R^{(P)} = -i\frac{\mu\bar{D}(\omega)}{4\pi\rho\omega^2}\,k_\alpha^3\sin^2\theta\sin 2\phi\,\frac{d}{dR}\,h_2^{(2)}(k_\alpha R)$$

$$\bar{u}_\theta^{(P)} = -i\frac{\mu\bar{D}(\omega)}{4\pi\rho\omega^2}\,k_\alpha^3\sin 2\theta\sin 2\phi\,\frac{h_2^{(2)}(k_\alpha R)}{R}$$

$$\bar{u}_\phi^{(P)} = -i\frac{\mu\bar{D}(\omega)}{2\pi\rho\omega^2}\,k_\alpha^3\sin\theta\cos 2\phi\,\frac{h_2^{(2)}(k_\alpha R)}{R}\,. \tag{38}$$

S-wave:

$$\bar{u}_R^{(S)} = -\frac{3i\mu\bar{D}(\omega)}{4\pi\rho\omega^2}\,k_\beta^3\sin^2\theta\sin 2\phi\,\frac{h_2^{(2)}(k_\beta R)}{R}$$

$$\bar{u}_\theta^{(S)} = -\frac{i\mu\bar{D}(\omega)}{8\pi\rho\omega^2}\,k_\beta^3\sin 2\theta\sin 2\phi\left[\frac{d}{dR}\,h_2^{(2)}(k_\beta R)+\frac{h_2^{(2)}(k_\beta R)}{R}\right]$$

$$\bar{u}_\phi^{(S)} = -\frac{i\mu\bar{D}(\omega)}{4\pi\rho\omega^2}\,k_\beta^3\sin\theta\cos 2\phi\left[\frac{d}{dR}\,h_2^{(2)}(k_\beta R)+\frac{h_2^{(2)}(k_\beta R)}{R}\right] \tag{39}$$

where

$$h_2^{(2)}(k_v R) = \frac{\exp(-ik_v R)}{ik_v R}\left\{\left[1-\frac{3}{(k_v R)^2}\right]-i\frac{3}{(k_v R)}\right\} \tag{40a}$$

and

$$\frac{d}{dR}\,h_2^{(2)}(k_v R) = -\frac{\exp(-ik_v R)}{R}\left\{\left[1-\frac{9}{(k_v R)^2}\right]-i\left[\frac{4}{k_v R}-\frac{9}{(k_v R)^3}\right]\right\} \tag{40b}$$

TIME DOMAIN SPHERICAL DISPLACEMENTS

Using equations (40) and inverting equations (38) and (39), we have for the *P*- and *S*-wave spherical displacements

P-wave:

$$u_R^{(P)} = \frac{1}{4\pi\rho}\,\frac{1}{\alpha^3}\sin^2\theta\sin 2\phi\mu\left\{\frac{\dot{D}(t-R/\alpha)}{R}+\frac{4\alpha}{R^2}\,D(t-R/\alpha)+\frac{9\alpha^2}{R^3}\,E(t-R/\alpha)+\frac{9\alpha^3 G(t-R/\alpha)}{R^4}\right\}$$

$$u_\theta^{(P)} = -\frac{1}{4\pi\rho}\,\frac{1}{\alpha^2}\sin 2\theta\sin 2\phi\mu\left\{\frac{D(t-R/\alpha)}{R^2}+\frac{3\alpha E(t-R/\alpha)}{R^3}+\frac{3\alpha^2 G(t-R/\alpha)}{R^4}\right\}$$

$$u_\phi^{(P)} = -\frac{1}{2\pi\rho}\,\frac{1}{\alpha^2}\sin\theta\cos 2\phi\mu\left\{\frac{D(t-R/\alpha)}{R^2}+\frac{3\alpha E(t-R/\alpha)}{R^3}+\frac{3\alpha^2 G(t-R/\alpha)}{R^4}\right\} \tag{41}$$

S-wave:

$$u_R^{(S)} = -\frac{3}{4\pi\rho}\frac{1}{\beta^2}\sin^2\theta\sin 2\phi\mu\left\{\frac{D(t-R/\beta)}{R^2} + \frac{3\beta E(t-R/\beta)}{R^3} + \frac{3\beta^2 G(t-R/\beta)}{R^4}\right\}$$

$$u_\theta^{(S)} = \frac{1}{8\pi\rho}\frac{1}{\beta^3}\sin 2\theta\sin 2\phi\mu\left\{\frac{\dot{D}(t-R/\beta)}{R} + \frac{3\beta}{R^2}D(t-R/\beta) + \frac{6\beta^2 E(t-R/\beta)}{R^3} + \frac{6\beta^3 G(t-R/\beta)}{R^4}\right\}$$

$$u_\phi^{(S)} = \frac{1}{4\pi\rho}\frac{1}{\beta^3}\sin\theta\cos 2\phi\mu\left\{\frac{\dot{D}(t-R/\beta)}{R} + \frac{3\beta}{R^2}D(t-R/\beta) + \frac{6\beta^2 E(t-R/\beta)}{R^3} + \frac{6\beta^3 G(t-R/\beta)}{R^4}\right\} \tag{42}$$

where

$$\dot{D}(t) = \frac{dD}{dt} \quad \text{or} \quad \bar{\dot{D}}(\omega) = i\omega\bar{D}(\omega)$$

$$E(t) = \int_0^t D(\tau)\,d\tau \quad \text{or} \quad \bar{E}(\omega) \equiv \frac{\bar{D}(\omega)}{i\omega}$$

$$G(t) = \int_0^t E(\tau)\,d\tau \quad \text{or} \quad \bar{G}(\omega) \equiv \frac{\bar{D}(\omega)}{(i\omega)^2}$$

and we have assumed $D(t) = 0$ for $t < 0$.

The displacement field for the pure shear point dislocation or double couple at any orientation (δ, λ) can be written in a form similar to equations (41) and (42) with $\sin^2\theta\sin 2\phi$, $(\sin 2\theta/2)\sin 2\phi$, and $\sin\theta\cos 2\phi$ replaced by the orientation angle function $\mathscr{R}_R(\delta, \lambda)$, $\mathscr{R}_\theta(\delta, \lambda)$ and $\mathscr{R}_\phi(\delta, \lambda)$ respectively, which are given as functions of θ, ϕ, δ, and λ in Appendix C.

Equations (41) and (42) are of the same form as the Cartesian displacements due to a second order multipole given by Bessonova *et al.* (1960), p. 19. Similar results are given in Haskell (1969) in Cartesian tensor form.

For our dislocation or slip history we will use the following function preferred by Ohnaka (1973)

$$D(t) = \begin{cases} D_0[1-(1+k_T t)\exp(-k_T t)]; & t \geqslant 0 \\ 0 \quad ; & t < 0. \end{cases} \tag{43}$$

Even though this slip function is the solution of a critically damped mechanical system with static friction and a dynamic friction proportional to slip velocity, we have chosen it primarily for its convenience and not its physical significance. It has the advantage of yielding under certain fault geometries far-field seismic displacements previously proposed in the literature.

A frequently discussed fault model is a finite rectangular surface in the (x_1, x_3) plane over which a constant dislocation propagates unilaterally in the x_1 direction with constant rupture velocity, v_0 and instantaneous rupture in the x_3 direction. For this simple fault

model at far-field observer positions defined by the direction cosines $\gamma_3 = 0$ and $\gamma_1 = \alpha/v_0$ for *P*-waves and $\gamma_3 = 0$ and $\gamma_1 = \beta/v_0$ for *S* waves, the far-field body wave displacement time history is given by the derivative of equation (43), i.e. $\sim k_T^2 t \exp(-k_T t)$, which is the history proposed by Brune (1970) and Berckhemer & Jacob (1968). This is also the far-field displacement contribution of each areal double couple on a more general fault surface involving shear slip only.

At fault–observer orientations for which the Haskell (1964) and Savage (1972) solutions are valid, the dislocation history, equation (43), results in a far-field displacement of a type favoured by Savage (1972) in that its spectral asymptotic behaviour is ω^{-3} and its initial displacement is proportional to t^2, i.e. displacement proportional to dislocation history.

The time functions corresponding to the derivatives and multiple integrals of equation (43), which are used in displacement-field solutions, equations (41) and (42), are

$$\dot{D}(t) = D_0 k_T^2 t \exp(-k_T t); \qquad t \geqslant 0$$

$$E(t) = \frac{D_0}{k_T}\{2\exp(-k_T t) + k_T t[1 + \exp(-k_T t)] - 2\}; \qquad t \geqslant 0$$

and

$$G(t) = \frac{D_0}{2k_T^2}\{6[1 - \exp(-k_T t)] + k_T t[k_T t - 4 - 2\exp(-k_T t)]\}; \qquad t \geqslant 0 \tag{44}$$

where the above functions are zero for $t < 0$.

The Fourier transform of this slip model is

$$\bar{D}(\omega) = \frac{k_T^2 D_0}{i\omega(k_T + i\omega)^2}. \tag{45}$$

The far-field displacements for the area double couples on the fault surface are given by

$$\bar{u}_R = \frac{1}{4\pi}\frac{\beta^2}{\alpha^3}\mathscr{R}_R(\delta, \lambda)\, i\omega\bar{D}(\omega)\,\frac{\exp(-ik_\alpha R)}{R}$$

$$\bar{u}_\theta = \frac{1}{4\pi}\frac{1}{\beta}\mathscr{R}_\theta(\delta, \lambda)\, i\omega\bar{D}(\omega)\,\frac{\exp(-ik_\beta R)}{R}$$

$$\bar{u}_\phi = \frac{1}{4\pi}\frac{1}{\beta}\mathscr{R}_\phi(\delta, \lambda)\, i\omega\bar{D}(\omega)\,\frac{\exp(-ik_\beta R)}{R} \tag{46}$$

which when combined with equation (45) yield an 'ω-square model' (Aki 1967). Of the infinite class of 'ω-square models', this is the minimum phase model, i.e. the time function with the most rapid build-up of energy.

Mixed quadrupole source

The second seismic source presented in this paper is what we shall call the 'mixed quadrupole source'. It is essentially a double couple in which the *P*-wave potential has a different time function or spectrum than the shear-wave potentials. All other factors in the potentials are the same as the double couple which has the same time function or spectrum, except for constant amplitude factors involving body velocities for both *P*- and *S*-wave potentials, e.g. equations (36).

The example presented here is the Archambeau (1972) model of a tectonic release source. In particular, we will restrict our discussion to the seismic radiation from a tectonic release or relaxation due to the instantaneous formation of a spherical cavity of radius R_0 centred in a spherical source medium of radius R_s initially under an applied constant pure shear stress. The pre-stressed source region is imbedded in an infinite unstressed elastic whole space with the same elastic properties as the pre-stressed spherical-source region. The final stress distribution in the source region, $R_0 \leqslant R < R_s$, is assumed to be that due to a spherical cavity in an elastic space under pure shear stress at infinity. For simplicity, we will assume that the initial constant shear stress is oriented so that all shear-stress components except $\sigma_{12}^{(0)}$ are zero.

From Archambeau (1972), the radiated spectral potentials under these assumptions are

$$\bar{\Phi} = -\frac{3}{2}\sigma_{12}^{(0)}\frac{1}{k_\alpha^2}\mathscr{F}_\alpha \sin^2\theta \sin 2\phi h_2^{(2)}(k_\alpha R)$$

$$\bar{\psi}_1 = -\frac{3}{2}\sigma_{12}^{(0)}\frac{1}{k_\beta^2}\mathscr{F}_\beta \cos\theta \sin\theta \cos\phi h_2^{(2)}(k_\beta R)$$

$$\bar{\psi}_2 = \frac{3}{2}\sigma_{12}^{(0)}\frac{1}{k_\beta^2}\mathscr{F}_\beta \cos\theta \sin\theta \sin\phi h_2^{(2)}(k_\beta R)$$

$$\bar{\psi}_3 = \frac{3}{2}\sigma_{12}^{(0)}\frac{1}{k_\beta^2}\mathscr{F}_\beta \sin^2\theta \cos 2\phi h_2^{(2)}(k_\beta R) \tag{47}$$

where

$$\mathscr{F}_\alpha = 5\frac{1}{(7-5\sigma)(\lambda+\mu)}\mathscr{B}_\alpha \qquad \mathscr{F}_\beta = 5\frac{\alpha^2}{\beta^2}\frac{1}{(7-5\sigma)(\lambda+\mu)}\mathscr{B}_\beta \tag{48}$$

and σ is Poisson's ratio.

For observers outside the source region, i.e. $R > R_s$

$$\mathscr{B}_v = \left(\frac{R_0}{v}\right)\left[\mathscr{D}(k_v R_0) - \left(\frac{R_0}{R_s}\right)^2 \mathscr{D}(k_v R_s)\right]$$

where

$$\mathscr{D}(x) = \cos x - \frac{\sin x}{x}.$$

For an observer inside the source region, i.e. $R_0 < R < R_s$ (Minster 1973)

$$\mathscr{B}_v = \frac{R_0}{v}\mathscr{D}(k_v R_0).$$

This is the same seismic radiation that an observer would detect if R_s were taken to be infinite (Randall 1966, 1973a, b; Minster 1973). It is due to the assumptions that the radiation from stress relaxation outside R_s is negligible and that the final stress distribution inside R_s is the stress field for pure shear at infinity. In obtaining equations (47), we have used the following relations between Archambeau's (1972) potentials, $\tilde{\chi}_j$ and ours

$$\tilde{\chi}_j = \frac{k_\beta^2}{2}\bar{\psi}_j \qquad j = 1, 2 \text{ and } 3$$

and

$$\tilde{\chi}_4 = -k_\alpha^2 \bar{\Phi}.$$

Since the R, θ, and ϕ dependence of equations (47) are the same as the horizontal double couple equations (36), we can obtain by inspection of equations (38), (39), (41) and (42) the corresponding displacements in the frequency and time domain

P-wave:

$$\bar{u}_R^{(P)} = K_\alpha \sin^2\theta \sin 2\phi \frac{d}{dR} h_2^{(2)}(k_\alpha R)$$

$$\bar{u}_\theta^{(P)} = K_\alpha \sin 2\theta \sin 2\phi \frac{h_2^{(2)}(k_\alpha R)}{R}$$

$$\bar{u}_\phi^{(P)} = 2K_\alpha \sin\theta \cos 2\phi \frac{h_2^{(2)}(k_\alpha R)}{R}. \tag{49}$$

S-wave:

$$\bar{u}_R^{(S)} = 3K_\beta \sin^2\theta \sin 2\phi \frac{h_2^{(2)}(k_\beta R)}{R}$$

$$\bar{u}_\theta^{(S)} = \frac{1}{2} K_\beta \sin 2\theta \sin 2\phi \left[\frac{d}{dR} h_2^{(2)}(k_\beta R) + \frac{h_2^{(2)}(k_\beta R)}{R}\right]$$

$$\bar{u}_\phi^{(S)} = K_\beta \sin\theta \cos 2\phi \left[\frac{d}{dR} h_2^{(2)}(k_\beta R) + \frac{h_2^{(2)}(k_\beta R)}{R}\right] \tag{50}$$

where

$$K_v \equiv -\frac{3}{2} \sigma_{12}^{(0)} \frac{1}{k_v^2} \mathscr{F}_v$$

or

$$K_v = -\frac{15}{2} \sigma_{12}^{(0)} \frac{(\lambda+2\mu)}{(7-5\sigma)(\lambda+\mu)} \frac{R_0^3}{\rho v} \left[\frac{\mathscr{D}(k_v R_0)}{\omega^2 R_0^2} - \frac{\mathscr{D}(k_v R_s)}{\omega^2 R_s^2}\right] \tag{51a}$$

for $R > R_s$, and

$$K_v = -\frac{15}{2} \sigma_{12}^{(0)} \frac{(\lambda+2\mu)}{(7-5\sigma)(\lambda+\mu)} \frac{R_0^3}{\rho v} \frac{\mathscr{D}(k_v R_0)}{\omega^2 R_0^2} \tag{51b}$$

for $R_0 < R < R_s$.

As pointed out by Randall (1973b) and Minster (1973) for $\omega \to 0, K_v = 0(\omega^2)$ for $R > R_s$ and $K_v = 0(1)$ for $R_0 < R < R_s$. Thus for the observer located in the pre-stressed field, the 'far-field' displacement spectrum is flat for long periods. The 'far-field' spectral displace-

ments due to a spectral moment, $\bar{M}(\omega)$, are given by

$$\bar{u}_R^{(P)} = -i\,\frac{\omega\bar{M}(\omega)}{4\pi\rho}\,\frac{1}{\alpha^3}\,\sin^2\theta\,\sin 2\phi\,\frac{d}{dR}\,h_2^{(2)}(k_\alpha R)$$

$$\bar{u}_\theta^{(S)} = -i\,\frac{\omega\bar{M}(\omega)}{8\pi\rho}\,\frac{1}{\beta^3}\,\sin 2\theta\,\sin 2\phi\left[\frac{d}{dR}\,h_2^{(2)}(k_\beta R) + \frac{h_2^{(2)}(k_\beta R)}{R}\right]$$

$$\bar{u}_\phi^{(S)} = -i\,\frac{\omega\bar{M}(\omega)}{4\pi\rho}\,\frac{1}{\beta^3}\,\sin\theta\,\cos 2\phi\left[\frac{d}{dR}\,h_2^{(2)}(k_\beta R) + \frac{h_2^{(2)}(k_\beta R)}{R}\right]$$

where the seismic moment, M_0, is given by

$$M_0 = \lim_{\omega\to 0}\,|\omega\bar{M}(\omega)|.$$

Comparing with equations (49), (50) and (51b) and taking the limit as $\omega \to 0$, $R < R_s$, we find that the seismic moment for both *P*- and *S*-wave displacements is the same and is equal to

$$M_0 = 10\pi\sigma_{12}^{(0)}\,\frac{(\lambda+2\mu)}{(7-5\sigma)(\lambda+\mu)}\,R_0^3 \tag{52}$$

where we have used the limit relation

$$\frac{\mathscr{D}(k_v R_m)}{\omega^2 R_m^2} \to \frac{1}{3}\left(-\frac{1}{v^2} + \frac{\omega^2 R_m^2}{10v^4}\right); \qquad \omega \ll 1.$$

For a Poisson solid, i.e. $\lambda = \mu$, the seismic moment is

$$M_0 = \frac{60}{23}\,\pi R_0^3\,\sigma_{12}^{(0)}$$

which is the value given by Randall (1973a) and Aki & Tsai (1972).

TIME DOMAIN SPHERICAL DISPLACEMENTS

Transforming equations (49) and (50) into the time domain, we obtain expressions for the displacement field similar to expressions (41) and (42) with $(1/4\pi\rho)(\mu/v^2)$ replaced by vL_v and the time histories $\dot{D}$, D, E and G replaced by $\dot{D}^{(v)}$, $D^{(v)}$, $E^{(v)}$ and $G^{(v)}$, respectively, where

$$L_v = -\frac{15}{2}\,\sigma_{12}^{(0)}\,\frac{(\lambda+2\mu)}{(7-5\sigma)(\lambda+\mu)}\,\frac{R_0^3}{\rho v}$$

$$\dot{D}^{(v)}(t) = \frac{C_0^{(v)}(t)}{R_0^2} - \frac{C_s^{(v)}(t)}{R_s^2}; \qquad R > R_s$$

$$C_m^{(v)}(t) = \frac{1}{2\pi}\int_{-\infty}^{\infty}\bar{C}_m^{(v)}(\omega)\exp(i\omega t)\,d\omega; \qquad m = 0 \text{ or } s$$

$$\bar{C}_m^{(v)}(\omega) = \frac{1}{(i\omega)^2}\,\mathscr{D}(k_v R_m)$$

$$C_m^{(\upsilon)}(t) = \begin{cases} 0; & t \leqslant t' \\ \frac{1}{2}(t-t')\,[1-(\upsilon/R_m)(t-t')/2]; & t' \leqslant t \leqslant t'' \\ 0; & t \geqslant t'' \end{cases} \tag{53}$$

$t' = -R_m/\upsilon$ and $t'' = R_m/\upsilon$.

As before the other time histories are multiple time integrals of $\dot{D}^{(\upsilon)}$ and υ is either α or β depending on whether the displacements are *P*- or *S*-waves respectively.

The above relations are for the observer range $R > R_s$. For $R_0 < R < R_s$ we set R_s finite, e.g.

$$\dot{D}^{(\upsilon)}(t) = \frac{\dot{D}_0^{(\upsilon)}(t)}{R_0^2}\,.$$

The latter results from Archambeau's formulation, which insures no internal reflections at the R_s boundary. Thus an observer inside of R_s does not know the boundary exists.

These relations are appropriate for the instantaneous formation of the cavity of radius R_0 at time $t = 0$. If the cavity is generated from the origin at a constant rupture velocity of $V_R > \alpha$, the spectral relations should be modified by a phase delay of $\omega R_0/V_R$ and the time relations by an origin time delay of R_0/V_R. For V_R less than the body velocities, the spectral and time histories are changed depending on whether $\alpha > V_R > \beta$ or $\beta > V_R$.

One of the disturbing features of Archambeau's source for $R > R_s$ is that information arrives at the observer from R_s travelling with the speed of a body velocity from an origin time of $t = 0$. This implies that the source position R_s is aware of the formation of the cavity at $t = 0$; a non-causal situation. Archambeau (private communication) feels that this early arrival is due to the initial condition that the pre-stress field is not at static equilibrium at R_s. It is his opinion that this early seismic radiation is from an initial relaxation of source position R_s to static equilibrium and is not related to relaxation due to the formation of a cavity in the finite pre-stress region.

Further examples of mixed quadrupole sources with references can be found in Molnar, Tucker & Brune (1973).

These displacements can also be generalized to those for an arbitrary pure shear field orientation by replacing $\sin^2\theta \sin 2\phi$, $(\sin 2\theta/2) \sin 2\phi$ and $\sin\theta \cos 2\phi$ with the orientation angle functions $\mathscr{R}_R(\delta, \lambda)$, $\mathscr{R}_\theta(\delta, \lambda)$ and $\mathscr{R}_\phi(\delta, \lambda)$, respectively.

Numerical examples

In this section we numerically present body-wave displacements due to a double-couple and to two mixed quadrupole sources. We will compare displacements at a set of distances from the sources to investigate criteria for estimating the minimum range at which near field terms can be neglected.

As previously mentioned, we will use the Ohnaka dislocation or slip history for our double couple model. In Fig. 2, we show the Ohnaka source, the Ben-Menahem & Toksoz (1963) source, and the Haskell (1964) source with their respective time constants as determined by the authors for a best fit to seismic-wave data from the Kamchatka earthquake of 1952, November 4. Also shown on the figure is the Randall–Archambeau, $R_0 < R < R_s$, equivalent time history adjusted to the same constant value for times greater than 30 s.

For the double couple or point-dislocation type sources, the Ben-Menahem & Toksoz and the Haskell time histories yield an ω^{-1} high-frequency asymptote and the Ohnaka time

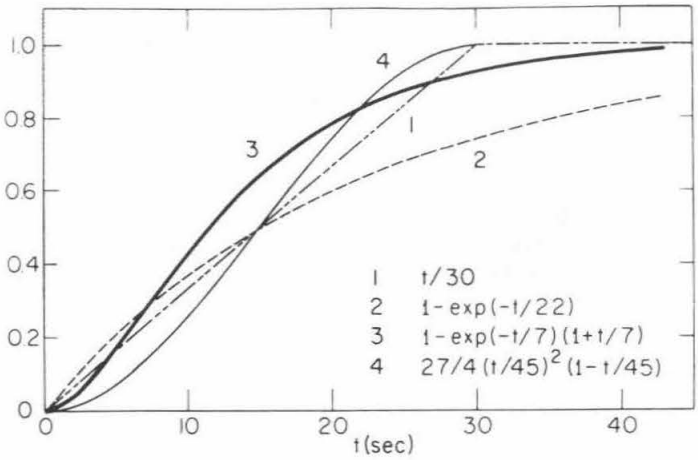

Figure 2. Dislocation time histories. (1) Hadkell 1964. (2) Ben-Menahem & Toksoz 1963. (3) Ohnaka 1973. (4) Randall–Archambeau equivalent history.

history yields an 'ω-square model'. For the long, narrow rectangular-fault model of Haskell, we have an ω^{-2} for the Ben-Menahem & Toksoz and the Haskell slip histories and an ω^{-3} fall-off for the Ohnaka slip history. The Archambeau and the Randall sources are ω^{-2} models for all observer positions.

From the form of our double-couple displacement fields, equations (41) and (42), it is not obvious that there is any range, R, for which the displacement field generated by a finite point dislocation will remain bounded with increasing time. This apparent discrepancy with far-field results is caused by the $1/R^3$ and $1/R^4$ near-field terms which contains first and second time integrals of the dislocation history. A similar situation for the spectrum of the near-field Archambeau solution was discussed by Minster (1973). He found that the apparent anomaly is resolved when the total spectral displacement field is considered.

If we consider the total displacement field given by the sum of equations (41) and (42), we find that any bounded point, shear-dislocation history results in a bounded total displacement field. In particular, if the dislocation history reaches a constant value, D_0, after a given time, t_0, we have for $t > t_0$

$$\dot{D}(t) = 0, \qquad D(t) = D_0$$

$$E(t) = D_0 t + a, \qquad G(t) = \frac{D_0 t^2}{2} + at + b$$

$$u_R^s \equiv u_R^{(P)} + u_R^{(S)}; \qquad t > t_0 + R/\beta$$

$$= \frac{1}{8\pi} \frac{(3\lambda + 5\mu)}{(\lambda + 2\mu)} \frac{D_0}{R^2} \mathscr{R}_R(\delta, \lambda) \tag{54a}$$

$$u_\xi^s \equiv u_\xi^{(P)} + u_\xi^{(S)}; \qquad t > t_0 + R/\beta$$

$$= \frac{1}{4\pi} \frac{\mu}{(\lambda + 2\mu)} \frac{D_0}{R^2} \mathscr{R}_\xi(\delta, \lambda) \tag{54b}$$

where the subscript ξ denotes θ or ϕ and

where a and b are constants of integration which do not enter into the final displacement field. Equations (54) can also be obtained from spectral equations (38) and (39) by using the limit relation

$$u^s = \lim_{\omega \to 0} \{i\omega[\bar{u}^{(p)} + \bar{u}^{(s)}]\}$$

Even though equations (54) have the classical $(1/R^2)$ dependence, this dependence results from the combination of $(1/R)$ through $(1/R^4)$ terms in the dynamic field expressions, i.e. equations (41) and (42), and cannot be obtained from their $(1/R^2)$ terms alone.

In the far field, the peak values, as determined by the maximum of the $(1/R)$ terms in equations (41) and (42), are for the Ohnaka history

$$\{u_R^f\}_{\max} = \frac{1}{4\pi} \frac{\beta^2}{\alpha^3} \frac{k_T D_0}{eR} \mathscr{R}_R(\delta, \lambda)$$

$$\{u_\xi^f\}_{\max} = \frac{1}{4\pi} \frac{1}{\beta} \frac{k_T D_0}{eR} \mathscr{R}_\xi(\delta, \lambda) \tag{55}$$

These peak values occur at a time $T_0 = 1/k_T$ after the P and S arrival times.

In Figs 3 and 4, radial- and transverse-displacement histories are shown at various ranges from the Ohnaka point shear dislocation. The scaled displacements u_R^* and u_θ^* in the figures

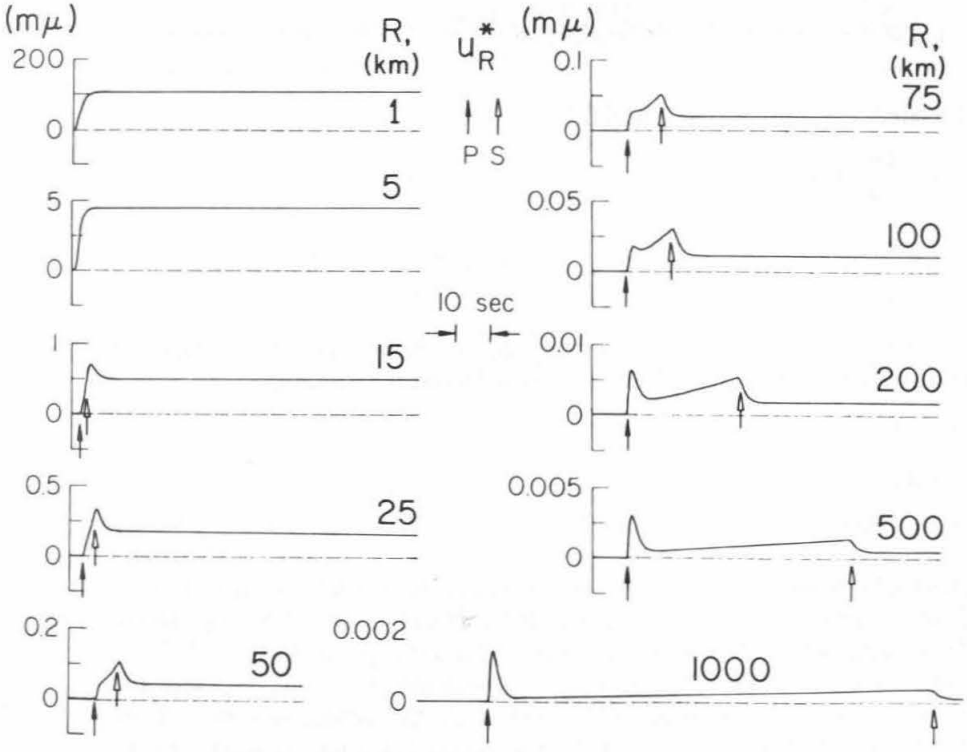

Figure 3. Scaled radial displacements at various ranges for an Ohnaka dislocation history. P- and S-wave arrival times are indicated by the letters P and S, respectively.

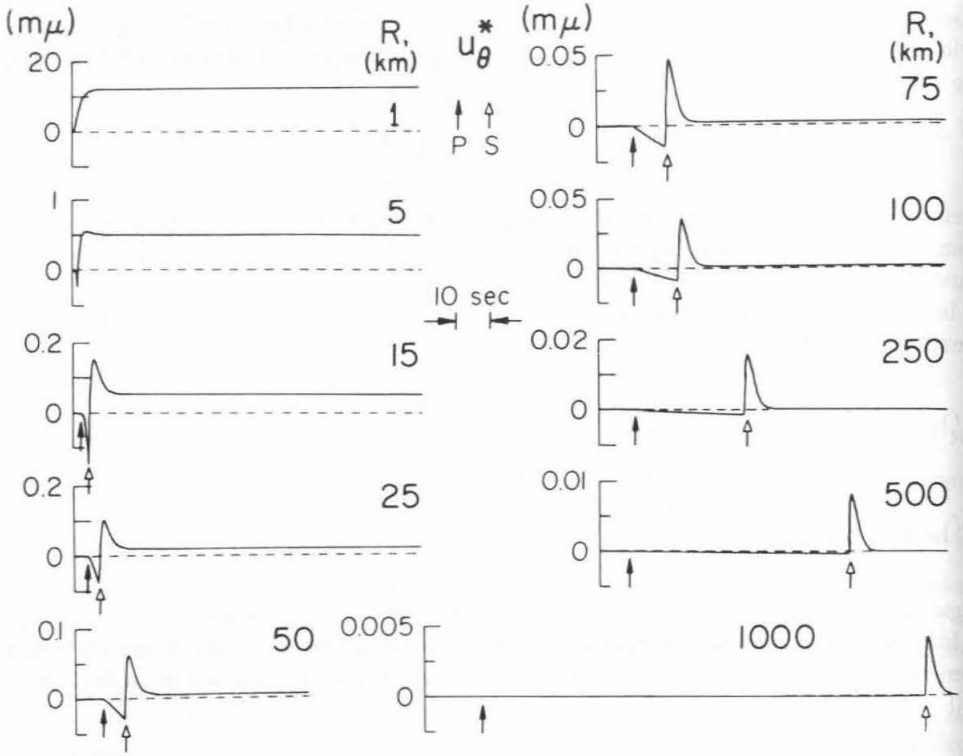

Figure 4. Scaled tangential displacements at various ranges for Ohnaka dislocation history.

are related to the displacement field by

$$u_R = \frac{\mu D_0}{4\pi\rho} \mathscr{R}_R(\delta, \lambda)\, u_R^*$$

$$u_\xi = \frac{\mu D_0}{2\pi\rho} \mathscr{R}_\xi(\delta, \lambda)\, u_\theta^* . \tag{56}$$

The far-field peak displacement rise-time, T_0, for these figures is 1 s. For a different T_0, the range, time scale, and amplitude of the displacement field scale as

$$R = T_0 R_F$$

$$t = T_0 t_F \tag{57}$$

$$A = (1/T_0)^2 A_F$$

respectively, where R_F, t_F, and A_F are the values shown on the figures. As an example, the u_R^* at $R = 15$ km in Fig. 3 is the u_R^* at $R = 1.5$ km for a $T_0 = 0.1$ s with the time scale of 10 s changed to 1 s and the amplitude scale of 1 μm changed to 100 μm.

One of the objectives of this study is to estimate the minimum range for which the far-field term is an appropriate representation of the displacement field. In Figs 3 and 4, we see that the displacement field at small ranges has a history similar to the source or dislocation history. The far-field maximum for u_R^* does not emerge from the onset displacement as a recognizable feature until ranges between 50 and 100 km for $T_0 = 1$ s. Even

though a peak value for u_θ^* is apparent at ranges between 5 and 10 km, it is not a good estimate of the far-field maximum until at ranges greater than 50 km. At 25 km, the peak value is only about 75 per cent of the far-field maximum.

For both u_R^* and u_θ^* the near-field displacement field rises to a peak value and then approaches the static displacement value with increasing time. For u_R^* the peak value is greater than the far-field or $(1/R)$ maximum and for u_θ^* it is less. One estimate, suggested by the figures, of the minimum range for which the far-field approximation is adequate would be that the far-field displacement be appreciably larger than the static displacement. From equations (54) and (55), we have

$$\frac{\{u_R^f\}_{\max}}{u_R^s} = \frac{2\beta^2}{\alpha(3\alpha^2 - \beta^2)} \frac{R}{T_0 e}$$

$$\frac{\{u_\xi^f\}_{\max}}{u_\xi^s} = \frac{\alpha^2}{\beta^3} \frac{R}{T_0 e}. \tag{58}$$

The elastic parameters used for the figures are $\alpha = 6.3$ km s^{-1} and $\beta = 3.5$ km s^{-1}. For a ratio of at least 10, we would have a minimum range of 747 km for radial displacements and 30 km for tangential displacements.

It should be remembered that equations (41) and (42) and the results shown in Figs 3 and 4 are the displacement field contributions from the pure shear point dislocations on the fault surface and must be integrated over the fault surface to obtain the displacement field.

From plane models with only minor variations in areal dislocation strength and history and at observer orientations for which the travel-time variation over the fault dimensions is small compared to the far-field signal duration, the displacement field can be represented by equations (41) and (42) multiplied by the fault area, e.g. Helmberger (1973). For these models D_0 is the area averaged relative displacement over the fault. We then can rewrite equations (54) and (55) in terms of the seismic moment, M_0, where

$$M_0 = \mu D_0 A_R,$$

and A_R is the area of the fault surface.

For observations and faults where these relations are applicable, we can estimate the moment, M_0, in the time domain from the peak displacement and the peak rise-time, T_0. An easier estimate of T_0 is the half-width of the peak displacement and is related to T_0 for the Ohnaka history by

$$T_0 = \frac{\Delta T_{1/2}}{2.44}$$

The half-width, $\Delta T_{1/2}$, is the time interval from 1/2 the maximum displacement on one side of the peak to 1/2 the maximum displacement on the other side. In terms of these variables the moment is

$$M_0 = 4\pi\rho\alpha^3 R \frac{1}{\mathscr{R}_R(\delta, \lambda)} (1.11)\, \Delta T_{1/2} \{u_R^f\}_{\max}$$

$$M_0 = 4\pi\rho\beta^3 R \frac{1}{\mathscr{R}_\xi(\delta, \lambda)} (1.11)\, \Delta T_{1/2} \{u_\xi^f\}_{\max}. \tag{59}$$

The amplitude values shown in Figs 3 and 4 are the displacements for a moment of $M_0 = 10^{16}$ dyne cm when scaled by the directivity and specific density, ρ.

Although equations (59) are valid only for the far-field, moments were calculated from the displacements in Figs 3 and 4. The moments calculated from the near-field radial displacements are larger than the actual moment, the smaller the range the greater the difference. For example, the calculated moments are 1.55×10^{16}, 1.25×10^{16} and 1.12×10^{16} dyne cm at ranges of 250, 500 and 1000 km, respectively. At the illustrated ranges of 100 km and less, the far-field shape has not separated enough from the near field to measure a half-width. It was possible to calculate moments from the tangential displacements at illustrated ranges of 15 km and greater. For ranges of 15, 25 and 50 km, the measured moments are 0.79×10^{16}, 0.76×10^{16} and 0.90×10^{16} dyne cm, respectively. At ranges of 75 km and greater the moments are essentially 1×10^{16} dyne cm. Even though the observed moments from the near-field tangential displacements are less than the actual moments, they give a considerably better estimate in the near-field than radial displacements.

As mentioned earlier these distances are proportional to T_0, which is the far-field displacement rise time. T_0 of 1 s is appropriate for large earthquakes, so that these minimum ranges should be considered an upper limit for most earthquakes.

Time-domain estimates of moment suffer from uncertainties similar to those inherent in spectral estimates of moment such as directivity, propagation corrections back to the focal sphere, and instrument response. In addition, equations (59) are based on assumptions concerning source phase as well as amplitude spectrum. If it were not for the fact that the next source we will consider yields moment relations approximately the same as equations (59), the preceding discussion on moments would be purely academic. For completeness, the spectral corner frequency for the Ohnaka dislocation history is related to the half-width $\Delta T_{1/2}$ by

$$f_c = \frac{1}{2\pi T_0} = \frac{0.389}{\Delta T_{1/2}}$$

Of our two examples of a mixed quadrupole source, we will consider first numerically the Randall or Archambeau, $R_0 < R < R_S$, tectonic release model which we will refer to as the Randall source model. The results from this source can be easily extended to the Archambeau, $R > R_S$ displacement fields.

The static- or long-time displacement field for this source is

$$u_R^s = \frac{L_\alpha}{6\alpha\beta^2} \frac{1}{R^2} \left\{(3\alpha^2 - \beta^2) - \frac{9}{5} \frac{R_0^2}{R^2} (\alpha^2 - \beta^2)\right\} \mathscr{R}_R(\delta, \lambda)$$

$$u_\xi^s = \frac{L_\beta}{3\alpha^2\beta} \frac{1}{R^2} \left\{\beta^2 + \frac{3}{5} \frac{R_0^2}{R^2} (\alpha^2 - \beta^2)\right\} \mathscr{R}_\xi(\delta, \lambda). \tag{60}$$

The far-field peak values are

$$\{u_R^f\}_{\max} = \frac{L_\alpha}{4} \frac{1}{\alpha R_0 R} \mathscr{R}_R(\delta, \lambda)$$

$$\{u_\xi^f\}_{\max} = \frac{L_\beta}{4} \frac{1}{\beta R_0 R} \mathscr{R}_\xi(\delta, \lambda). \tag{61}$$

The peak values occur at times $T_0^{(\alpha)} = R_0/\alpha$ and $T_0^{(\beta)} = R_0/\beta$ after the P and S arrival times from the nearest point of the cavity, respectively. The static- and far-field peak values can be expressed in terms of the tectonic release seismic moment given in equation (52) by the

substitution

$$L_v = -\frac{3M_0}{4\pi\rho}\frac{1}{v}.$$

For $R \gg R_0$, the static displacements, in terms of moment, M_0, reduce to those of the point dislocation, except for their sign. The difference in sign is due to the tectonic release definition of moment, in that the sense of displacement from a release of positive $\sigma_{12}^{(0)}$ is opposite to our imposed positive dislocation $D(t)$.

In Figs 5 and 6, radial and transverse displacement histories are shown at various ranges for the Randall tectonic release model. The scaled displacements in the figures are related to the displacement field by

$$u_R = -\frac{3M_0}{4\pi\rho}\mathscr{R}_R(\delta, \lambda)\, u_R^*$$

$$u_\xi = -\frac{3M_0}{2\pi\rho}\mathscr{R}_\xi(\delta, \lambda)\, u_\theta^*. \tag{62}$$

The cavity radius, $R_0 = 6.3$ km, was chosen so that the far-field peak-rise time for P-waves, $T_0^{(\alpha)}$, in these figures is 1 s. The range, time scale, and amplitude of the displacement fields shown in Figs 5 and 6 scale as equations (57) with T_0 replaced by $T_0^{(\alpha)}$.

For the purpose of obtaining far-field range criteria, we note that the displacements for this source have many features in common with those from the Ohnaka dislocation. Similar

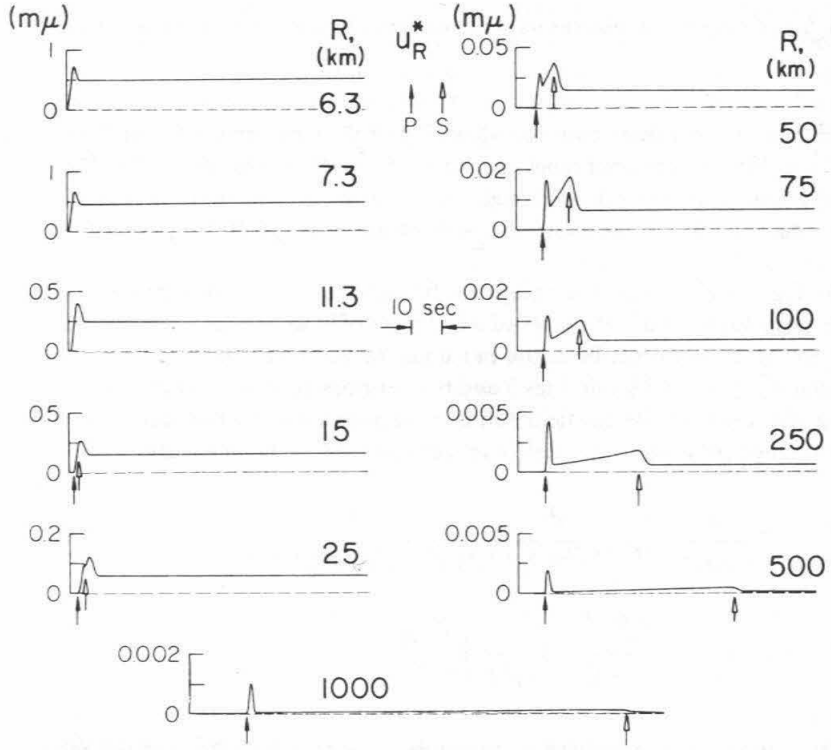

Figure 5. Scaled radial displacements at various ranges for a Randall–Archambeau mixed quadrupole.

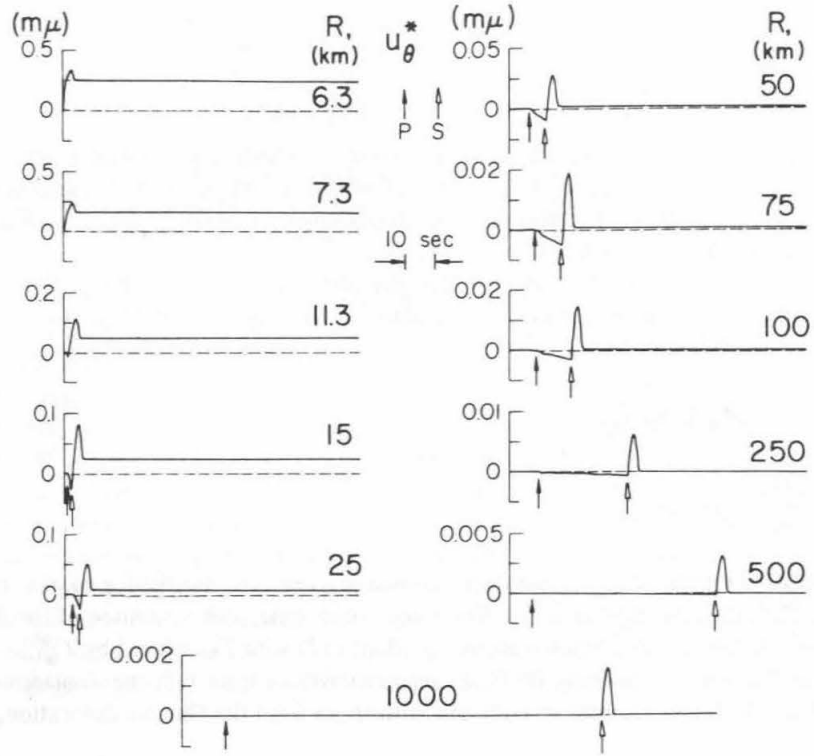

Figure 6. Scaled tangential displacements at various ranges for a Randall–Archambeau mixed quadrupole.

to Fig. 3, the far-field maximum for u_R^* in Fig. 5 does not emerge from the onset displacement as a useful feature until ranges between 25 and 50 km for $T_0^{(\alpha)} = 1$ s. The 'onset-glitch' before the displacement peak at a range of 25 km which becomes the far-field maximum at greater ranges would overestimate the peak value of the $(1/R)$ term by a factor of two to three.

As in Fig. 4, u_θ^* in Fig. 6 develops far-field characteristics at much smaller ranges than u_R^*. The peak value of u_θ^* at ranges of 11–15 km only underestimates the peak value of the $(1/R)$ term by 25 per cent. Both the radial and tangential displacements of the cavity walls, i.e. u_R^* and u_θ^* at $R = 6.3$ km in Figs 5 and 6, overshoot then return to their static values.

Using the ratio of the far-field terms maximum value to the static displacement as a minimum range criterion for far-field applicability we have from equations (60) and (61)

$$\frac{\{u_R^f\}_{\max}}{u_R^s} = 2\,\frac{\beta^2}{\alpha\{(3\alpha^2-\beta^2) - 9/5(R_0/R)^2\,(\alpha^2-\beta^2)\}}\left[\frac{3R}{4T_0^{(\alpha)}}\right]$$

$$\frac{\{u_\xi^f\}_{\max}}{u_\xi^s} = \frac{\alpha^2}{\beta\{\beta^2 + 3/5(R_0/R)^2(\alpha^2-\beta^2)\}}\left[\frac{3}{4}\,\frac{R}{T_0^{(\beta)}}\right] \tag{63}$$

For a ratio of 10, we would have a minimum range of 366 km for radial displacements and 28 km for tangential displacements.

The half-width of the peak displacement, $\Delta T_{1/2}^{(v)}$, for this source is related to $T_0^{(v)}$ by

$$T_0^{(v)} = \frac{\Delta T_{1/2}^{(v)}}{\sqrt{2}} \tag{64}$$

which yields the following time-domain estimates of the seismic moment

$$M_0 = -4\pi\rho\alpha^3 R \frac{1}{\mathscr{R}_R(\delta, \lambda)} (0.943)\, \Delta T_{1/2}^{(\alpha)} \{u_R^f\}_{\max}$$

$$M_0 = -4\pi\rho\beta^3 R \frac{1}{\mathscr{R}_\xi(\delta, \lambda)} (0.943)\, \Delta T_{1/2}^{(\beta)} \{u_\xi^f\}_{\max} \tag{65}$$

and the corner frequencies by

$$f_c^{(v)} = \frac{\sqrt{3}}{2\pi T_0^{(v)}} = \frac{0.390}{\Delta T_{1/2}^{(v)}}.$$

When scaled by the directivity and the specific density, ρ, i.e. by equations (62), the amplitude values shown in Figs 5 and 6 are the displacements for a moment of $M_0 = 10^{16}$ dyne cm.

The displacements in Figs 5 and 6 were used in equations (65) to obtain estimates of this moment. As with the Ohnaka point dislocation, the moment values calculated from the near-field radial displacements are larger than the actual moment, the smaller the range the greater the difference. For example, the estimated moments at range of 1000, 250 and 75 km were 1.17×10^{16}, 1.31×10^{16} and 1.40×10^{16} dyne cm respectively. At the illustrated ranges of less than 75 km, it was not possible to measure a half width related to the far-field peak. For the tangential displacements, it was possible to determine a half-width for ranges in Fig. 6 down to 15 km. The estimated moments at ranges of 250, 50 and 15 km were 0.96×10^{16}, 0.83×10^{16} and 0.66×10^{16} dyne cm, respectively. Again the tangential displacement estimates of the moment are better than the radial displacement estimates.

For the Archambeau tectonic release model, $R > R_s$, the static or long-time displacement field can be obtained by subtracting equations (60) with R_0 replaced by R_s from equations (60). This results directly from comparison of equation (51a) with (51b). The far-field peak values are obtained similarly.

Since the time integral of the far-field displacements is zero or equivalently the far-field displacement spectrum is zero at zero frequency, this source has no moment in the classical sense. As far as practical measurement is concerned, one can estimate a moment using equation (65). Since most seismometers have a limited long-period response, one's ability to differentiate between no moment and moment sources in the frequency or time domain is questionable.

Figs 7 and 8 give displacement histories for the Archambeau model at $R > R_s$. The cavity radius is $R_0 = 0.63$ km and the pre-stress radius is $R_s = 6.3$ km which results in a $T_0^{(\alpha)} = 0.1$ s. Thus for comparison of near-field effects between the Randall and Archambeau sources we should compare Randall model histories in Figs 5 and 6 with Archambeau model histories in Figs 7 and 8 at ranges and time scales ten times smaller. For an example the displacement histories at $R = 100$ km in Figs 7 and 8 should be compared with displacement histories in Figs 5 and 6 at $R = 1000$ km. And even though it is true that near-field effects such as the static displacement fall off as $(1/R^4)$ for the Archambeau model compared to $(1/R^2)$ for the Randall model and the shear dislocation model, the displacement histories in Figs 7 and 8 at

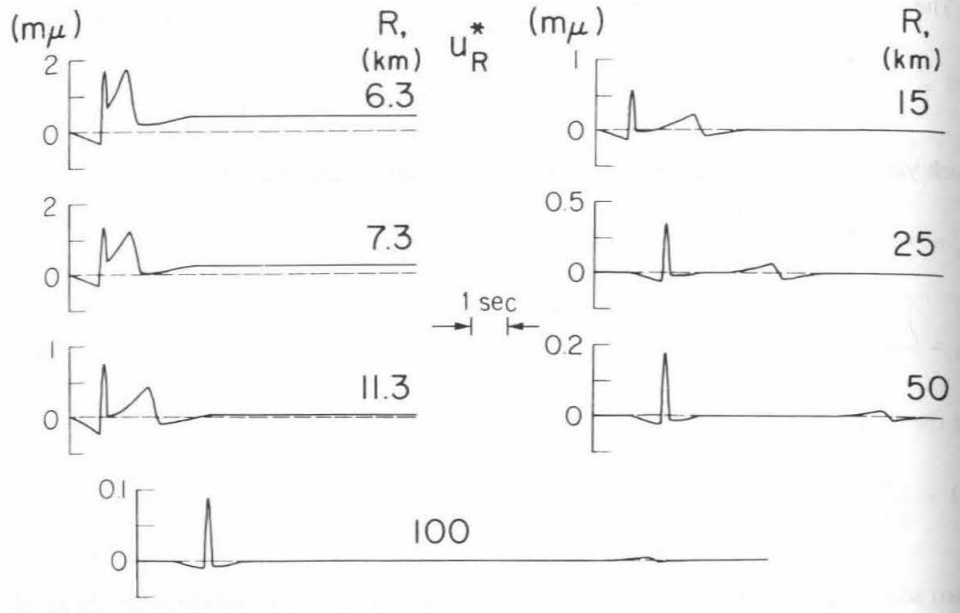

Figure 7. Scaled radial displacements at various ranges for an Archambeau mixed quadrupole.

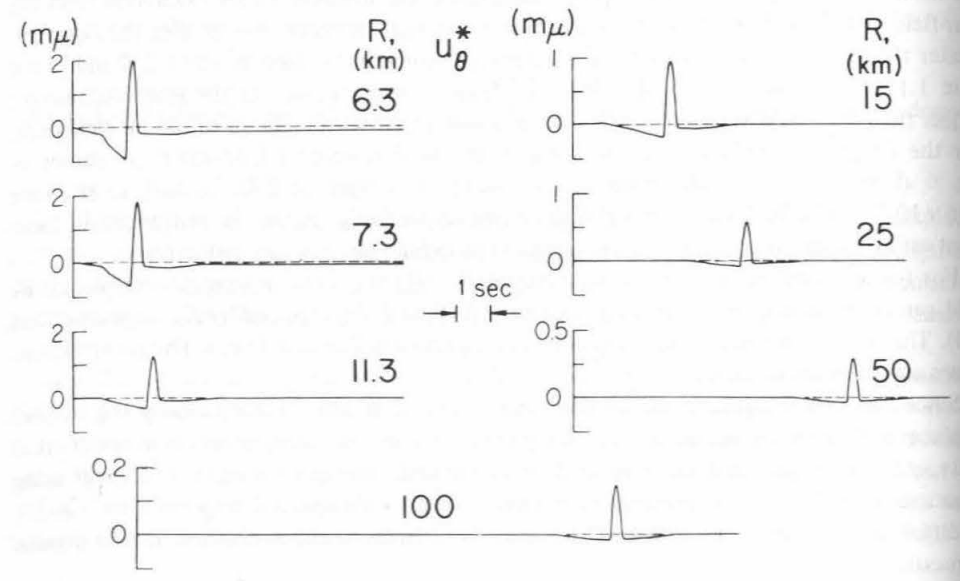

Figure 8. Scaled tangential displacements at various ranges for an Archambeau mixed quadrupole.

say $R = 7.3$ km are not that much different from the displacement histories at $R = 75$ km in Figs 5 and 6 after proper time scaling.

The last displacement histories in Figs 5 and 6 and the last histories in Figs 7 and 8 demonstrate one difficulty in determining actual moments. The difference between the no moment model of Figs 7 and 8 and the moment source of Figs 5 and 6 is the long-duration downwarp in Figs 7 and 8 due to R_s which cancels out the area under the pulse due to R_0 in

Figs 5 and 6. The larger R_s is to R_0 the smaller the amplitude of the down warp and the longer the duration compared to the R_0 pulse. Thus the larger R_s is to R_0, the more difficult it becomes to estimate the cancelling area due to R_s.

This assumes that one could obtain displacements for an actual event. The effect of some long-period seismic recording systems would be to take the positive area pulse in Figs 5 and 6 and superimpose a downwarp in order to cancel out the area similar to the effect shown in Figs 7 and 8. The basic difference would be that the downwarp for an instrument is causal and would not begin until the R_0 pulse arrived.

Comparison of equations (59) for the Ohnaka shear dislocation and equations (65) for the Randall tectonic release source suggests that a time-domain estimation of the moment using the peak far-field displacement value and its half-width duration defined by

$$M_0 = 4\pi\rho\alpha^3 R \frac{1}{\mathscr{R}_R(\delta, \lambda)} \Delta T_{1/2}^{(\alpha)} \{u_R^f\}_{\max}$$

$$M_0 = 4\pi\rho\beta^3 R \frac{1}{\mathscr{R}_\xi(\delta, \lambda)} \Delta T_{1/2}^{(\beta)} \{u_\xi^f\}_{\max} \tag{66}$$

and a corner frequency estimation by

$$f_c^{(v)} = \frac{0.39}{\Delta T_{1/2}^{(v)}} \tag{67}$$

might be appropriate for a wide variety of dislocation or equivalent dislocation histories. For the finite ramp or Haskell (1964) dislocation history equation (66) is appropriate for the moment but the corner frequency is given by

$$f_c = \frac{1}{\pi \Delta T_{1/2}} = \frac{0.318}{\Delta T_{1/2}}.$$

So far in this discussion, we have neglected the effect of fault–observer orientation on the far-field pulse width due to finite source dimensions. For a unilateral rectangular shear fault with an invariant, Haskell dislocation history and rupture velocity, the far-field source effect can be factored into three spectral terms. Each term is a function of one of three characteristic source duration times (Geller 1976). T_D is the ramp dislocation rise time. T_L and T_W are duration times associated with fault length and width respectively and are determined by fault geometry, body-wave velocity, rupture velocity, and position of the observer. For this simple finite fault model, $\Delta T_{1/2}^{(v)}$ is equal to the largest of the duration times if it is greater than the sum of the other two. The corner frequency given by the intersection of the $(1/\omega)$ asymptote with the flat part of the spectrum is related to $\Delta T_{1/2}^{(v)}$ by our last equation.

The above relations are not particularly surprising since the definition of seismic moment is related to the area under the far-field displacement history for which the product of the peak and the half-width is a measure of the area and the half-width of the displacement pulse is an indication of the frequency content of the signal. In fact, seismic moment is related to the area, S_i, under the far-field displacement, u_i^f, by

$$M_0 = 4\pi\rho\alpha^3 R \frac{S_R}{\mathscr{R}_R(\delta, \lambda)}$$

$$M_0 = 4\pi\rho\beta^3 R \frac{S_\xi}{\mathscr{R}_\xi(\delta, \lambda)}.$$

Similarly, we might also use the following compromise between equations (58) and equations (63)

$$\frac{\{u_R^f\}_{\max}}{u_R^s} = \frac{2\beta^2}{\alpha(3\beta^2-\beta^2)}\,\frac{R}{\Delta T_{1/2}^{(\alpha)}}$$

$$\frac{\{u_\xi^f\}_{\max}}{u_\xi^s} = \frac{\alpha^2}{\beta^3}\,\frac{R}{\Delta T_{1/2}^{(\beta)}}\,. \tag{68}$$

From our results on moment measurements in the time domain, ranges which correspond to a ratio of 10 in equation (68) can be used as an estimate of the minimum range of applicability of the far-field approximation. The particular value of the ratio is arbitrary and depends on the amount of error one is willing to accept. The minimum range for a corresponding error in assuming that the peak amplitude scales as $(1/R)$ is less than that for moment measurement. The moment sensitivity is caused by the static or near-field distortion of the pulse width relative to peak amplitude. The amount of pulse-width distortion carried over to the seismogram will depend on the instrument.

Thus what we would consider as estimates of the minimum ranges for the far-field approximation applied to time-domain moment calculations are from equations (68)

$$R_c^{(\alpha)} = \frac{5\alpha(3\alpha^2-\beta^2)}{\beta^2}\,\Delta T_{1/2}^{(\alpha)} \tag{69a}$$

for radial displacements and

$$R_c^{(\beta)} = \frac{10\beta^3}{\alpha^2}\,\Delta T_{1/2}^{(\beta)} \tag{69b}$$

for the transverse displacements.

Most far-field approximations are based on the spectral assumption of $k_\upsilon R \gg 1$, i.e. the observer is a large number of wavelengths from the source. Thus, it is interesting to see how our minimum distance criterion, equations (69), translates into a wavelength criterion for a source with a dominant frequency or wavelength. Two of our sources have no dominant wavelength but by definition, the corner frequency $f_c^{(\upsilon)}$ will be greater than any dominant source frequency. For both the Ohnaka and Randall source histories, $R_c^{(\upsilon)}$ corresponds to 17 and 1.2 wavelengths for P- and S-waves respectively at corner frequency wavelengths.

Another interesting frequency, $\omega_{DC}^{(\upsilon)}$, is that given by the intersection of the nearfield $(1/\omega)$ asymptote with the far-field spectral value for $\omega \ll 1$. For the Ohnaka and Randall histories, we have

$$\omega_{DC}^{(\alpha)} = \frac{(3\alpha^2-\beta^2)}{2\beta^2}\,\frac{\alpha}{R}$$

$$\omega_{DC}^{(\beta)} = \frac{\beta^2}{\alpha^2}\,\frac{\beta}{R}\,. \tag{70}$$

In terms of our source histories, this is the minimum frequency for which far-field theory can be used. In other words, for frequencies less than $f_{DC}^{(\upsilon)}$, there will be a significant near-field effect on the spectrum. Unfortunately, even frequencies greater than $f_{DC}^{(\upsilon)}$ may also be subject to near-field contamination. This frequency is only dependent on the elastic

constants and observer distance and not on source rise time or duration. For both *P*- and *S*-waves, $R_c^{(v)}$ yields the following ratio

$$\frac{f_c^{(v)}}{f_{DC}^{(v)}} = 20\pi T_{1/2}^{(v)} f_c^{(v)} \cong 24.5$$

for our chosen compromise relation between $T_{1/2}^{(v)}$ and $f_c^{(v)}$.

This discussion points out another advantage of defining $R_c^{(v)}$ in terms of half-pulse width or its spectral equivalent corner frequency. The ratio of corner frequency to near-field frequency $f_{DC}^{(v)}$ is independent of elastic medium and source rise time or duration for the Ohnaka and Randall source histories.

Conclusions

The theoretical results given in this paper for potentials and displacements can be used in a wide variety of elastodynamic problems involving seismic sources which are reduceable to quadrupoles or spatial integrals of quadrupoles.

Aside from the purely theoretical aspects of this paper, a comparison of displacement fields for the two types of seismic sources at various source distances suggested a criterion for determining the minimum range of the applicability of far-field solutions to the time domain. The criterion is based on the ratio of peak far-field displacement to the static field. Since the peak value depends on the source rise time, we have expressed the criterion in terms of some practical estimate of the rise time, e.g. the half peak width. For the three time histories considered, our criterion is conservative as to the minimum range for the $(1/R)$ dependence of peak amplitude as predicted by far-field results. On the other hand it is satisfactory for determining the minimum range for far-field based estimates of moment and corner frequency. Since the relative amount of static displacement effects the observed pulse width of body waves, it is not surprising that a criterion based on its significance would be most useful in moment- and corner-frequency estimates which are directly influenced by the signal's time distortion.

Our limited investigation of time histories suggested that approximate time domain estimates of the 'spectral corner frequency' can be obtained from a simple measurement of the half peak width. Even though the instrument will distort this value and its effect is easier to correct in the frequency domain, this estimate should be a valuable check on difficult or questionable spectral determinations where the time window by necessity may have included multiple arrivals. It should be especially useful in comparing the relative corner frequencies of *P*- and *S*-waves recorded on the same seismic record.

Acknowledgments

This research was supported by the Advanced Projects Agency of the Department of Defense and was monitored by the Air Force Office of Scientific Research under Contracts F44620-72-C-0078 and F44620-72-C-0083. Contribution No. 2660.

References

Aki, K., 1967. Scaling law of seismic spectrum, *J. geophys. Res.*, **72**, 1217–1231.

Aki, K. & Tsai, Y. B., 1972. Mechanism of Love-wave excitation by explosive sources, *J. geophys. Res.*, 77, 1452–1475.

Archambeau, C. B., 1972. The theory of stress wave radiation from explosions in prestressed media, *Geophys. J. R. astr. Soc.*, **29**, 329–366.

Ben-Menahem, A. & Toksoz, M. N., 1963. Source mechanism, from spectrums of long-period surface waves. 2. The Kamchatka earthquake of November 4, 1952, *J. geophys. Res.*, **68**, 5207–5222.

Ben-Menahem, A. & Singh, S. J., 1968. Eigenvector expansions of Green's dyads with applications to geophysical theory, *Geophys. J. R. astr. Soc.*, **16**, 417–452.

Berckhemer, H. & Jacob, K. H., 1968. Investigation of the dynamical process in earthquake foci by analyzing the pulse shape of body waves, *Final report*, Contract AF61(052)-801, 85 pp. Institute of Meteorology and Geophysics, University of Frankfurt, Germany.

Bessonova, E. N., Gotsadze, Keilis-Borok, V. I., Kirillova, I. V., Kogan, S. D., Kikhtikova, T. I. Malinovskaya, L. N., Pavlova, G. I. & Sorskii, A. A., 1960. *Investigation of the mechanism of earthquakes*, American Geophysical Union, Consultants Bureau, New York.

Brune, J. N., 1970. Tectonic stress and the spectra of seismic shear waves from earthquakes, *J. geophys. Res.*, **75**, 4997–5009.

Burridge, R., Lapwood, E. R. & Knopoff, L., 1964. First motions from seismic sources near a free surface, *Bull. seism. Soc. Am.*, **54**, 1889–1913.

Erdelyi, A., 1937. Zur theorie der kugelwellen, *Physica*, **4**, 107–102.

Erdelyi, A., Magmus, W., Oberhettinger, F. & Tricomi, F. G., 1954. *Tables of integral transforms*, vol. 1–2, Bateman Manuscript Project, California Institute of Technology, McGraw-Hill Book Company, New York.

Geller, R. J., 1976. Scaling relations for earthquake source parameters and magnitudes, *Bull. seism. Soc. Am.*, in press.

Haskell, N. A., 1964. Total energy and energy spectral density of elastic wave radiation from propagating faults, *Bull. seism. Soc. Am.*, **54**, 1811–1842.

Haskell, N. A., 1969. Elastic displacements in the near-field of a propagating fault, *Bull. seism. Soc. Am.*, **59**, 865–908.

Helmberger, D. V., 1974. Generalized ray theory for shear dislocations, *Bull. seism. Soc. Am.*, **64**, 45–64.

Minster, J. B., 1973. *Elastodynamics of failure in a continuum*, PhD thesis, California Institute of Technology, Pasadena.

Molnar, P., Tucker, B. E. & Brune, J. N., 1973. Corner frequencies of *P* and *S* waves and models of earthquake sources, *Bull. seism. Soc. Am.*, **63**, 2091–2104.

Ohnaka, M., 1973. A physical understanding of the earthquake source mechanism., *J. Phys. Earth*, **21**, 39–59.

Randall, M. J., 1966. Seismic radiation from a sudden phase transition, *J. geophys. Res.*, **71**, 5297–5302.

Randall, M. J., 1973a. Spectral peaks and earthquakes source dimension, *J. geophys. Res.*, **78**, 2609–2611.

Randall, J. M., 1973b. Low frequency spectra in seismic waves from explosions, *Geophys. J. R. astr. Soc.*, **32**, 387–388.

Sato, R., 1969. Formulations of solutions for earthquakes source models and some related problems, *J. Phys. Earth*, **11**, 101–110.

Sato, R., 1972. Seismic waves in the near field, *J. Phys. Earth*, **20**, 357–375.

Savage, J. C., 1965. The effect of rupture velocity upon seismic first motions, *Bull. seism. Soc. Am.*, **55**, 263–275.

Savage, J. C., 1974. Relation of corner frequency to fault dimensions, *J. geophys. Res.*, **77**, 3788–3795.

Takeuchi, H., 1966. *Theory of the Earth's interior*, p. 29, Blaisdell, Waltham, Massachusetts.

Appendix A

CYLINDRICAL DISPLACEMENTS AND POTENTIALS FOR A DOUBLE COUPLE OF ARBITRARY ORIENTATION

The transformation of the displacements given in equation (1) from the source coordinate system shown in Fig. 1 to cylindrical displacements in the epicentral cylindrical coordinate system yields

$$\begin{aligned}
\bar{q} &= -\frac{\bar{M}(\omega)}{4\pi\rho\omega^2}\{\sin\lambda\sin 2\delta U_3 + (\cos\lambda\cos\delta\cos\phi - \sin\lambda\cos 2\delta\sin\phi)\,U_2 \\
&\qquad + (\cos\lambda\sin\delta\sin 2\phi + \tfrac{1}{2}\sin\lambda\sin 2\delta\cos 2\phi)\,U_1\} \\
\bar{v} &= -\frac{\bar{M}(\omega)}{4\pi\rho\omega^2}\{-(\cos\lambda\cos\delta\sin\phi + \sin\lambda\cos 2\delta\cos\phi)\,V_2 \\
&\qquad + (\cos\lambda\sin\delta\cos 2\phi - \tfrac{1}{2}\sin\lambda\sin 2\delta\sin 2\phi)\,V_1\} \\
\bar{w} &= -\frac{\bar{M}(\omega)}{4\pi\rho\omega^2}\{\sin\lambda\sin 2\delta W_3 + (\cos\lambda\cos\delta\cos\phi - \sin\lambda\cos 2\delta\sin\phi)\,W_2 \\
&\qquad + (\cos\lambda\sin\delta\sin 2\phi + \tfrac{1}{2}\sin\lambda\sin 2\delta\cos 2\phi)\,W_1\}
\end{aligned} \tag{A1}$$

where

$$\begin{aligned}
U_1 &\equiv \frac{\partial}{\partial r}\left[\frac{\partial^2}{\partial r^2} - \frac{1}{r}\frac{\partial}{\partial r}\right](A_\beta - A_\alpha) + k_\beta^2\frac{\partial A_\beta}{\partial r} \\
V_1 &\equiv \frac{2}{r}\left[\frac{\partial^2}{\partial r^2} - \frac{1}{r}\frac{\partial}{\partial r}\right](A_\beta - A_\alpha) + k_\beta^2\frac{\partial A_\beta}{\partial r} \\
W_1 &\equiv \frac{\partial}{\partial z}\left[\frac{\partial^2}{\partial r^2} - \frac{1}{r}\frac{\partial}{\partial r}\right](A_\beta - A_\alpha)
\end{aligned} \tag{A2}$$

$$\begin{aligned}
U_2 &\equiv -\left[2\frac{\partial^3(A_\beta - A_\alpha)}{\partial^2 r\,\partial z} + k_\beta^2\frac{\partial A_\beta}{\partial z}\right] \\
V_2 &\equiv -\left[\frac{2}{r}\frac{\partial^2(A_\beta - A_\alpha)}{\partial r\,\partial z} + k_\beta^2\frac{\partial A_\beta}{\partial z}\right] \\
W_2 &\equiv -\left[2\frac{\partial^3(A_\beta - A_\alpha)}{\partial r\,\partial z^2} + k_\beta^2\frac{\partial A_\beta}{\partial r}\right]
\end{aligned} \tag{A3}$$

and

$$\begin{aligned}
U_3 &\equiv -\frac{1}{2}\left\{\frac{\partial}{\partial r}\left[\frac{\partial^2}{\partial r^2} - \frac{1}{r}\frac{\partial}{\partial r}\right](A_\beta - A_\alpha) - 2\frac{\partial^3}{\partial r\,\partial z^2}(A_\beta - A_\alpha) + k_\beta^2\frac{\partial A_\beta}{\partial r}\right\} \\
V_3 &\equiv -\frac{1}{2}\left\{\frac{2}{r}\left[\frac{\partial^2}{\partial r^2} - \frac{1}{r}\frac{\partial}{\partial r}\right](A_\beta - A_\alpha) + k_\beta^2\frac{\partial A_\beta}{\partial r}\right\} = -\frac{1}{2}V_1 \\
W_3 &\equiv -\frac{1}{2}\left\{\frac{\partial}{\partial z}\left[\frac{\partial^2}{\partial r^2} - \frac{1}{r}\frac{\partial}{\partial r}\right](A_\beta - A_\alpha) - 2\frac{\partial^3}{\partial z^3}(A_\beta - A_\alpha) - 2k_\beta^2\frac{\partial A_\beta}{\partial z}\right\}
\end{aligned} \tag{A4}$$

The integral relations (7) and (8) for the cylindrical potentials were obtained by substituting the Sommerfeld integral representation into equations (A1) for their respective (δ, λ) and comparing with the potential form, equation (4).

Noting that, for a given i in equations (A1), the orientation coefficients, i.e. terms involving λ, δ and ϕ, are identical for U_i and W_i and that the orientation coefficient for V_i is related to them by a simple derivative with respect to ϕ, we can group these coefficients with the coefficients of the integral relations for the cylindrical potentials given by equations (6), (7) and (8) to obtain the compact integral solutions for the potentials of a double couple of arbitrary orientation

$$\bar{\Phi} = \frac{\bar{M}(\omega)}{4\pi\rho\omega^2} \sum_{n=0}^{2} \Lambda_n \int_0^\infty A_n^0 F_\alpha J_n(kr)\, dk$$

$$\bar{\Psi} = \frac{\bar{M}(\omega)}{4\pi\rho\omega^2} \sum_{n=0}^{2} \Lambda_n \int_0^\infty B_n^0 F_\beta J_n(kr)\, dk \tag{A5}$$

$$\bar{X} = \frac{\bar{M}(\omega)}{4\pi\rho\omega^2} \sum_{n=0}^{2} \frac{\partial}{\partial\phi} \Lambda_n \int_0^\infty C_n^0 F_\beta J_n(kr)\, dk$$

where

$$\begin{aligned} \Lambda_0 &= \tfrac{1}{2} \sin\lambda \sin 2\delta \\ \Lambda_1 &= \cos\lambda \cos\delta \cos\phi - \sin\lambda \cos 2\delta \sin\phi \\ \Lambda_2 &= \tfrac{1}{2} \sin\lambda \sin 2\delta \cos 2\phi + \cos\lambda \sin\delta \sin 2\phi \end{aligned} \tag{A6}$$

and

$$\begin{aligned} &A_0^0 = k^2 + 2\nu_\alpha^2, \qquad A_1^0 = -2\epsilon k \nu_\alpha, \qquad A_2^0 = k^2 \\ &B_0^0 = 3\epsilon\nu_\beta \qquad B_1^0 = \frac{k_\beta^2 - 2k^2}{k}, \qquad B_2^0 = \epsilon\nu_\beta \\ &C_0^0 = 0, \qquad C_1^0 = \frac{\epsilon k_\beta^2 \nu_\beta}{k}, \qquad C_2^0 = -\frac{k_\beta^2}{2} \end{aligned} \tag{A7}$$

$$\epsilon = \operatorname{sgn}(z - h).$$

These are the same as the relations given by Sato (1972) except that his 'λ' is the negative of this λ.

In terms of the hypocentral spherical harmonics, the compressional and shear potentials in the source spherical coordinate system given in equation (36) can be expressed as

$$\begin{aligned} \bar{\Phi} &= -i \frac{\bar{M}(\omega)}{4\pi\rho\omega^2} \frac{k_\alpha^3}{3} \{6\Lambda_0 P_2^0(\cos\theta) - 2\Lambda_1 P_2^1(\cos\theta) + \Lambda_2 P_2^2(\cos\theta)\} h_2^{(2)}(k_\alpha R) \\ \bar{\psi}_1 &= -i \frac{\bar{M}(\omega)}{4\pi\rho\omega^2} \frac{k_\beta^3}{3} \left\{3 \frac{\partial\Lambda_0}{\partial\delta} P_2^0(\cos\theta) - \frac{\partial\Lambda_1}{\partial\delta} P_2^1(\cos\theta) + \frac{1}{2} \frac{\partial\Lambda_2}{\partial\delta} P_2^2(\cos\theta)\right\} h_2^{(2)}(k_\beta R) \\ \bar{\psi}_2 &= -i \frac{\bar{M}(\omega)}{4\pi\rho\omega^2} \frac{k_\beta^3}{3} \{3\Gamma_0 P_2^0(\cos\theta) - \Gamma_1 P_2^1(\cos\theta) + \tfrac{1}{2}\Gamma_2 P_2^2(\cos\theta)\} h_2^{(2)}(k_\beta R) \end{aligned} \tag{A8}$$

and

$$\bar{\psi}_3 = -i\,\frac{\bar{M}(\omega)}{4\pi\rho\omega^2}\,\frac{k_\beta^3}{3}\left\{\frac{\partial}{\partial\phi}\,\Lambda_1 P_2^1(\cos\theta) - \frac{1}{2}\,\frac{\partial}{\partial\phi}\,\Lambda_2 P_2^2(\cos\theta)\right\} h_2^{(2)}(k_\beta R)$$

where the Λ_i are defined earlier and

$\Gamma_0 = \cos\lambda\cos\delta$

$\Gamma_1 = \cos\lambda\sin\delta\sin\phi - \sin\lambda\sin 2\delta\cos\phi$

and

$\Gamma_2 = (\sin\lambda\cos 2\delta\sin 2\phi - \cos\lambda\cos\delta\cos 2\phi)$.

We can write equations (A6) in integral form using equation (34) and obtain

$$\bar{\Phi} = \frac{\bar{M}(\omega)}{4\pi\rho\omega^2}\sum_{n=0}^{2}\Lambda_n\int_0^\infty A_n^0 F_\alpha J_n(kr)\,dk$$

$$\bar{\psi}_1 = \frac{\bar{M}(\omega)}{4\pi\rho\omega^2}\sum_{n=0}^{2}\frac{\partial}{\partial\delta}\Lambda_n\int_0^\infty B_n^1 F_\beta J_n(kr)\,dk \qquad \text{(A7)}$$

$$\bar{\psi}_2 = \frac{\bar{M}(\omega)}{4\pi\rho\omega^2}\sum_{n=0}^{2}\Gamma_n\int_0^\infty B_n^2 F_\beta J_n(kr)\,dk$$

and

$$\bar{\psi}_3 = \frac{\bar{M}(\omega)}{4\pi\rho\omega^2}\sum_{n=0}^{2}\frac{\partial}{\partial\phi}\Lambda_n\int_0^\infty B_n^3 F_\beta J_n(kr)\,dk$$

where

$$A_0^0 = k^2 + 2\nu_\alpha^2, \qquad A_1^0 = -2\epsilon k\nu_\alpha, \qquad A_2^0 = k^2$$

$$B_0^1 = \frac{k^2 + 2\nu_\beta^2}{2}, \qquad B_1^1 = -\epsilon k\nu_\beta, \qquad B_2^1 = \frac{k^2}{2}$$

$$B_0^2 = \frac{k^2 + 2\nu_\beta^2}{2}, \qquad B_1^2 = -\epsilon k\nu_\beta, \qquad B_2^2 = \frac{k^2}{2} \qquad \text{(A8)}$$

$$B_0^3 = 0, \qquad B_1^3 = \epsilon k\nu_\beta, \qquad B_2^3 = -\frac{k^2}{2}$$

From equation (27), the B_n^3 are related to the C_n^0 of equation (A5) by

$$B_n^3 = \frac{k^2}{k_\beta^2}\,C_n^0$$

which is agreement with the results of equation (A8) and equations (A7).

The compressional and shear potentials solutions of this Appendix are for an arbitrary dislocation orientation. They are equally valid for the mixed quadrupole of arbitrary orientation with the replacement of the factor

$$\frac{\bar{M}(\omega)}{4\pi\rho\omega^2}$$

by the corresponding factors for the mixed quadrupole compressional and shear potentials.

Appendix B

RELATION BETWEEN CARTESIAN AND CYLINDRICAL VECTOR SHEAR POTENTIAL

Performing the curl of the displacement as defined in equations (17) and (19) and setting them equal, we have

$$\nabla(\nabla\cdot\bar{\psi}) - \nabla^2\bar{\psi} = (\nabla\cdot\tilde{\psi}) - \nabla^2\tilde{\psi} \tag{B1}$$

since

$$\nabla^2\bar{\psi} = -k_\beta^2\bar{\psi}$$

$$\nabla^2\tilde{\psi} = -k_\beta^2\tilde{\psi} \tag{B2}$$

$$\nabla\cdot\bar{\psi} = 0$$

and

$$\nabla\cdot\tilde{\psi} = \frac{\partial\tilde{\psi}_3}{\partial z}$$

equation (B1) becomes

$$\bar{\psi} = \tilde{\psi} + \frac{1}{k_\beta^2}\nabla\left(\frac{\partial\tilde{\psi}_3}{\partial z}\right) \tag{B3}$$

which is the vector form of equations (24).

Appendix C

ORIENTATION ANGLE FUNCTIONS

The spherical displacements for a dislocation in the source coordinate system (R, θ^0, ϕ^0), can be written as

$$\bar{u}_R^{0(\upsilon)} = F_R^{(\upsilon)} 2\gamma_1^0\gamma_2^0$$

$$\bar{u}_\theta^{0(\upsilon)} = \frac{1}{2}F_{\theta\phi}^{(\upsilon)}\, 4\,\frac{\gamma_1^0\gamma_2^0\gamma_3^0}{(\gamma_1^{02}+\gamma_2^{02})^{1/2}} = F_{\theta\phi}^{(\upsilon)}\,\frac{\partial(\gamma_1^0\gamma_2^0)}{\partial\theta^0}$$

$$\bar{u}_\phi^{0(\upsilon)} = F_{\theta\phi}^{(\upsilon)}\,\frac{(\gamma_1^{02}-\gamma_2^{02})}{(\gamma_1^{02}+\gamma_2^{02})^{1/2}} = F_{\theta\phi}^{(\upsilon)}\,\frac{1}{\sin\theta^0}\,\frac{\partial(\gamma_1^0\gamma_2^0)}{\partial\phi^0} \tag{C1}$$

where γ_i^0 are the direction cosines in the source coordinate system, the superscript υ is either P or S, and the function $F_R^{(\upsilon)}$ and $F_{\theta\phi}^{(\upsilon)}$ are defined implicitly by comparing equations (38) and (39) with (C1).

The displacements in the hypocentre spherical coordinate system (R, θ, ϕ), are

$$\bar{u}_R = \bar{u}_R^0$$

$$\bar{u}_\theta = \frac{\partial\theta^0}{\partial\theta}\,\bar{u}_\theta^0 + \sin\theta^0\,\frac{\partial\phi^0}{\partial\theta}\,\bar{u}_\phi^0 \tag{C2}$$

$$\bar{u}_\phi = \frac{1}{\sin\theta}\,\frac{\partial\theta^0}{\partial\phi}\,\bar{u}_\theta^0 + \frac{\sin\theta^0}{\sin\theta}\,\frac{\partial\phi^0}{\partial\phi}\,\bar{u}_\phi^0$$

and in combination with equations (C1), we have

$$\begin{aligned}
\bar{u}_R^{(v)} &= F_R^{(v)}\, 2\gamma_1^0\gamma_2^0 \\
\bar{u}_\phi^{(v)} &= F_{\theta\phi}^{(v)}\, \frac{\partial(\gamma_1^0\gamma_2^0)}{\partial\theta} \\
\bar{u}_\phi^{(v)} &= F_{\theta\phi}^{(v)}\, \frac{1}{\sin\theta}\, \frac{\partial(\gamma_1^0\gamma_2^0)}{\partial\phi}\,.
\end{aligned} \tag{C3}$$

The direction cosines of the source coordinate system are given in terms of the hypocentral spherical coordinate system as

$$\begin{aligned}
\gamma_1^0 &= \cos\lambda \sin\theta \cos\phi - \cos\delta \sin\lambda \sin\theta \sin\phi - \sin\delta \sin\lambda \cos\theta \\
\gamma_2^0 &= \sin\delta \sin\theta \sin\phi - \cos\delta \cos\theta
\end{aligned} \tag{C4}$$

We can now define the orientation angle functions by

$$\begin{aligned}
\mathscr{R}_R(\delta,\lambda) &\equiv 2\gamma_1^0\gamma_2^0 \\
\mathscr{R}_\theta(\delta,\lambda) &\equiv \frac{\partial}{\partial\theta}(\gamma_1^0\gamma_2^0) \\
\mathscr{R}_\phi(\delta,\lambda) &\equiv \frac{1}{\sin\theta}\frac{\partial}{\partial\phi}(\gamma_1^0\gamma_2^0)
\end{aligned} \tag{C5}$$

and from equations (C4), the orientation angle functions can be written as

$$\begin{aligned}
\mathscr{R}_R(\delta,\lambda) &= \cos\lambda\,\{\sin\delta\,\sin^2\theta\,\sin 2\phi - \cos\delta\,\sin 2\theta\,\cos\phi\} \\
&\quad + \sin\lambda\,\{\sin 2\delta\,(\cos^2\theta - \sin^2\theta\,\sin^2\phi) + \cos 2\delta\,\sin 2\theta\,\sin\phi\} \\
\mathscr{R}_\theta(\delta,\lambda) &= \cos\lambda\left\{\sin\delta\,\frac{\sin 2\theta}{2}\,\sin 2\phi - \cos\delta\,\cos 2\theta\,\cos\phi\right\} \\
&\quad - \sin\lambda\left\{\sin 2\delta\,\frac{\sin 2\theta}{2}\,(1+\sin^2\phi) - \cos 2\delta\,\cos 2\theta\,\sin\phi\right\} \\
\mathscr{R}_\phi(\delta,\lambda) &= \cos\lambda\,\{\sin\delta\,\sin\theta\,\cos 2\phi + \cos\delta\,\cos\theta\,\sin\phi\} \\
&\quad + \sin\lambda\left\{\cos 2\delta\,\cos\theta\,\cos\phi - \frac{\sin 2\delta}{2}\,\sin\theta\,\sin 2\phi\right\}
\end{aligned} \tag{C6}$$